Journal of Materials Chemistry C

ROYAL SOCIETY OF CHEMISTRY

REVIEW

View Article Online
View Journal | View Issue

Cite this: J. Mater. Chem. C, 2022, 10, 2475

Recent progress in pyrazinacenes containing nonbenzenoid rings: synthesis, properties and applications

Fangyuan Kang, [a] Jie Yang[a] and Qichun Zhang *[ab]

Received 11th September 2021,
Accepted 1st January 2022

DOI: 10.1039/d1tc04340d

rsc.li/materials-c

Azaacenes have emerged as a new and important class of organic materials, and their synthesis strategies and applications as organic semiconductors have gained significant progress in recent years. Generally, adopting sterically-shielding substituents such as attaching large silylethynyl groups at selected peripheral positions or extending the π-conjugation with pyrene units is the common method used to stabilize larger azaacenes. However, another way to stabilize and enlarge azaacenes, as well as to tune their optical and electronic properties by inserting nonbenzenoid rings such as four-membered rings into the skeletons, has also been developed but has received much less attention. Therefore, in this review, we summarize the recent progress in their syntheses, properties, and applications in organic electronics. Moreover, we highlight the effect of nonbenzenoid units in the systems. Finally, we discuss the current challenges and perspectives through comparison with conventional azaacenes.

1. Introduction

Acenes, consisting of linearly fused phenyl rings, have received remarkable research interest and success as active materials in various optoelectronic devices.[1–3] For example, naphthalene-substituted anthracene derivatives have been well developed as suitable emitting materials for full-color organic electroluminescent devices with highly efficient and stable blue emission,[4] while a monocrystalline rubrene derivative displays a hole mobility as high as 40 $cm^2 V^{-1} s^{-1}$.[5] Currently, one of the main issues frustrating preparative chemists and materials scientists is their poor stability in air or under light, especially for those skeletons larger than pentacene,[6,7] which also limits their further applications in devices. Incorporating sp^2 nitrogen atoms into the backbone of acenes leads to so-called azaacenes, and has been reported to be an effective way to stabilize the scaffolds,[8] increase their electron affinity and improve electron transport properties,[9,10] as well as decrease the degree of synthetic difficulty by simple condensation reactions[11–13] or Pd-mediated coupling reactions,[14,15] *etc.*[16–18] However, the critical issue of stability has still not been thoroughly resolved in higher systems, even when combined with different stabilization concepts such as purely steric loading, electronegative substitution, or physical methods.[19]

[a] *Department of Materials Science and Engineering, City University of Hong Kong, Hong Kong, SAR 999077, P. R. China. E-mail: qiczhang@cityu.edu.hk*
[b] *Center of Super-Diamond and Advanced Films (COSDAF), City University of Hong Kong, Hong Kong, SAR 999077, P. R. China*

Fangyuan Kang

Fangyuan Kang received his Masters degree from Chengdu Institute of Organic Chemistry, Chinese Academy of Sciences in 2015. He is a PhD candidate in Prof. Qichun Zhang's group, City University of Hong Kong. His research interests include the design, synthesis, and applications of carbon-rich nanomaterials and crystalline covalent organic networks.

Jie Yang

Jie Yang received his BS and PhD degrees from the School of Chemistry and Chemical Engineering, Huazhong University of Science and Technology in 2014 and 2019, respectively. He is now working as a postdoctoral fellow in Prof. Qichun Zhang's group, City University of Hong Kong. His research interests include the synthesis and applications of novel covalent organic frameworks and conjugated polymers.

Alternatively, introducing nonbenzenoid rings such as four-membered cyclobutadiene (CBD) into conjugated skeletons has been recently demonstrated as an intriguing method to extend the length of π-conjugation and simultaneously increase the stability accounting for the increase of the degree of Clar aromatic sextets.[20] This is very important because a larger but stable π-backbone not only favors the intermolecular π–π stacking in solid states but promises a facilely reversible oxidation to its radical cation, thus resulting in their better performance in organic electronics.[18] Moreover, the intrinsic non/anti-aromaticity of nonbenzenoid rings leads to the reduced aromaticity of the whole system, resulting in varied HOMO–LUMO energy levels with a reduced band gap,[16,21] enhanced conductance,[22] and tailored fluorescence.[23] Unfortunately, this category of molecules is presently not as popular as their singly annulated homologues in terms of synthesis strategies and applications. Considering their many desirable behaviors, a timely review on their advances is essential and very important.

Here, this review focuses on the synthesis methods, properties, and applications in devices beyond this group of untypical azaacenes. We firstly introduce azaacenes containing a four-membered ring and systematically compare the influence of the inserted cyclobutadiene ring on the resulting materials, then we provide an introduction of azaacenes bearing a five-membered ring. To access the four-membered-ring fused azaacenes, apart from using the classic condensation reactions and Pd-mediated coupling reactions, new methods approaching novel structures include the intramolecular condensation of privileged precursors[24] and Pd-mediated arene-oxanorbornene annulation (CANAL).[23] Similarly, the newly developed strategy of ruthenium-catalyzed butadiene-mediated benzannulation allows a quick synthesis of azaacenes bearing a five-membered ring with high yields.[25] We also include several interesting azaacenes bridged by macrocycles (≥7-membered ring) and highlight their size-dependent properties. It is worth pointing out that some selected molecules in this review may not be as ordered as those formally well-defined (aza)acenes[26–37] due to the diverse scaffolds and irregular shapes of the embedded units. Nevertheless, we aim to understand how the inclusion of these unusual rings in azaacenes can modulate their properties and subsequently affect their performance in devices. In addition, due to the small reorganization energies, attractive ionization potentials, favorable FMO energies,[38] *etc.*,[39] pyrazine-containing azaacenes, also called pyrazinacenes, are becoming the main representatives and receiving the most extensive research interest. Thereby the untypical structures pertaining to this review are also only complementary to those of quinoxaline-type azaacenes.

Qichun Zhang

Dr Qichun Zhang obtained his BS at Nanjing University in China in 1992, MS in physical organic chemistry (organic solid lab) at the Institute of Chemistry, Chinese Academy of Sciences in 1998, MS in organic chemistry at University of California, Los Angeles (USA), and completed his PhD in chemistry at the University of California Riverside in 2007. Then, he joined Prof. Kanatzidis' group at Northwestern University as a Postdoctoral Fellow (Oct. 2007–Dec. 2008). In Jan. 2009, he joined the School of Materials Science and Engineering at Nanyang Technological University (NTU, Singapore) as an Assistant Professor. On Mar 1st, 2014, he was promoted to Associate Professor with tenure. On Sept 1st 2020, he moved to the Department of Materials Science and Engineering at the City University of Hong Kong as a tenured full professor. Currently, he is an associate editor of J. Solid State Chemistry, an International Advisory Board member of Chemistry – An Asian Journal, an Advisory board member of Journal of Materials Chemistry C, an Advisory board member of Materials Chemistry Frontiers, an Advisory board member of Inorganic Chemistry Frontiers, an Advisory board member of Aggregate, and an Advisory board member of Materials Advances. In 2018, 2019, 2020 and 2021, he was recognized as a highly-cited researcher (top 1%) in the cross-field in Clarivate Analytics. He is a fellow of the Royal Society of Chemistry. Currently, his research focuses on carbon-rich conjugated materials and their applications. To date, he has published >445 papers and 5 patents (H-index: 95).

2. Azaacenes bearing a four-membered cyclobutadiene (CBD) ring

Incorporating four-membered cyclobutadiene units into azaacenes has been proven to be a useful method to enlarge and stabilize the backbone of azaacenes.[40] Based on the position of cyclobutadiene rings and pyrazine rings in the backbone, they can be structurally divided into three families within different basic building units. Accordingly, different synthetic strategies are adopted (Fig. 1). In the case of an **A**-type structure interspersing the cyclobutadiene ring in the backbone, the syntheses are often specifically modified from those approaches developed for the construction of classic azaacenes. The critical step is to build up the pyrazine ring, which has predominantly been fulfilled either by condensation of suitable *ortho*-quinones with *o*-diaminoarene precursors in acidic conditions[41,42] or through the Buchwald–Hartwig coupling between *ortho*-dihalide-arenes and aromatic *ortho*-diamines,[20,43] followed with/without an additional aromatization procedure. Alternatively, CANAL developed by Teo *et al.* is another effective method to approach CBD-containing azaacenes.[23] For the **C**-type structure in which two pyrazine rings directly flank the cyclobutadiene unit, the generally applicable approach is through the intramolecular condensation of the precursor squaric 1,3-diamidine, then aromatized by smooth oxidation with O_2.[24,44] Otherwise, note that the synthesis of a **B**-type structure juxtaposing CBD with pyrazine rings in the skeleton proceeds with a similar

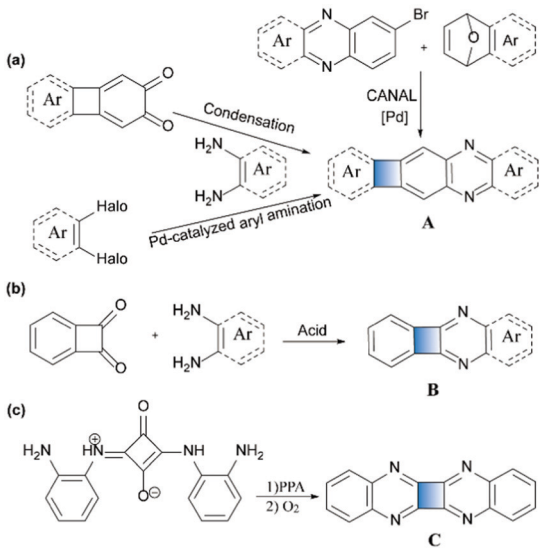

Fig. 1 A retrosynthetic analysis to construct **A**, **B**, and **C**-type skeletons.

acid-promoted condensation reaction, but this type of structure is rare apart from some early examples.[45–47]

In 1962, Blatchly *et al.* synthesized the first unsubstituted biphenylene-containing azaacene **3a** through a reaction between biphenylene-2,3-quinone and *o*-phenylenediamine in acetic acid.[48] The as-prepared yellow needles were only characterized by melting point and elemental analysis at that time. Not until 2015 did the Bunz group follow this work, simultaneously obtaining three new biphenylene-containing azaacenes **3b–d** with tri(^{iso}propylsilyl)ethynyl (TIPS-ethynyl) substitutions (Scheme 1a).[41] Interestingly, the condensation reaction involving biphenylene-2,3-quinone **1** gave the corresponding oxidized forms directly with high yields (68–84%); this was not observed during the synthesis of their relatives **3′** when using *ortho*-benzoquinone as one of the precursors, where only the *N*,*N*′-dihydro intermediates were obtained under this condition.[49] This was attributed to the anti-aromatic property of CBD in the system leading to the much higher energy of hydrogenation (−16.7 *vs.* −26.7 kcal mol^{-1} for compounds **3d** and **3d′**, respectively). However, as shown in Scheme 1b, their further exploration was demonstrated when the condensation reaction was conducted between **1** and phenazinodiamine **4**. The yield of product **5** dramatically dropped to only 18%.[42] In addition, more challenging species of symmetrically bibenzocyclobutadiene end-capped tetraazapentacenes **9a–b** were also synthesized *via* sequential condensation reactions by the same group (Scheme 1c).[42] Surprisingly, the overall yield of the three steps for target **9a** was two times higher than that of the congener **9b**, substantiating that the steric substitutions at the periphery could significantly influence the stability of synthetic

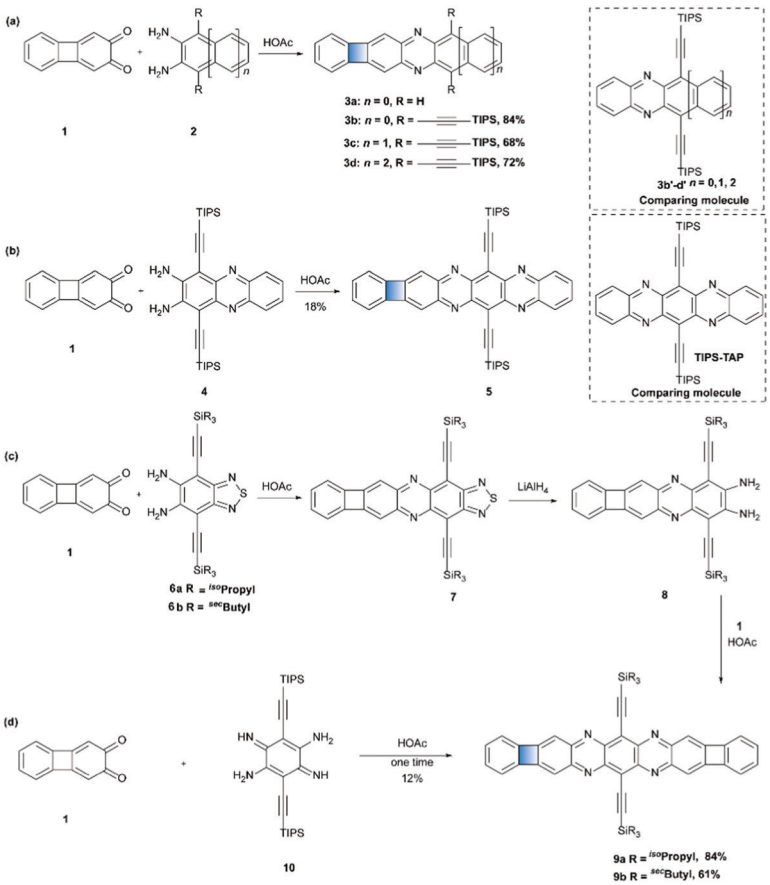

Scheme 1 Construction of biphenylene-containing azaacenes **3a–d**, **5** and **9a–b**.

intermediates and the resultant azaacenes. Alternatively, **9a** could also be obtained by a stepwise coupling between **1** and the diaminoimine **10** in an acceptable yield (Scheme 1d). Apparent redshifts in ultraviolet-visible (UV/Vis) absorption and emission spectra were observed as the enlarging of acene subunits. The maximal absorption bands for **3b–c** were 450 nm, 540 nm, and 650 nm, respectively. On the other hand, compared with the corresponding classic azaacenes **3′/TIPS-TAP**, the longest absorption wavelength showed a blue shift by 30–40 nm per added benzocyclobutadiene group. Moreover, the biphenylene substitution almost had no impact on the general electrochemical behavior. NICS-calculations suggested that only those benzene rings near the four-membered rings showed the reduced aromaticity, and the aromaticity of the remaining benzene rings was not influenced by the typical π, *zz*-values of −23 to −34 ppm as the benzene rings in common larger arenes are (Fig. 2a). In all, the aromaticity of the whole molecule was reduced, but it did not compromise the stability of the resulting skeletons, and all the materials exhibited enhanced stability in solid states. Meanwhile, the reduced aromaticity led to the destabilization of the LUMO, which considerably shifted compared with the corresponding classic counterparts. Quantum chemical calculations demonstrated that the HOMO was situated on the heteroacene motif, while the LUMO was distributed over the whole π-system (Fig. 2b), and the unequal distribution suggested their potential n-type semiconductor behaviors. However, the unfavorable stacking modes in the solid state may thwart them as ideal charge transporting materials. Compounds **3b–d** and **9a** adopted isolated one-dimensional stacks while compound **5** was arranged in a brick wall motif without any interlocking within layers in their single crystals (Fig. 2c).

In 1972, Hermann Pütter constructed an aza analogue of biphenylene **16a** *via* the intramolecular condensation of squaric 1,3-diamidine **15a**,[24,44] followed by a smooth oxidation with O_2. Interestingly, the central CBD was stabilized by two flanked pyrazine rings. Halogenation is a successful strategy to tailor electronic features and π–π stacking modes, thereby improving the electron transporting ability in n-type organic semiconductors.[50] Taking advantage of this, in 2015, Yang *et al.*[51] followed Pütter's approach with a slight modification to synthesize a group of chlorinated analogues **16b–f** (Scheme 2a). It is worth noting that the cyclization precursor **15**, arising from an amine exchange between (chloro)-*o*-phenylenediamine **14** and intermediate **13**,[24] was a complicated mixture. Thereby, the regioisomers **16d** and **16e** were also mixed. All compounds showed good thermal stability in the air even when heated up to 250 °C. The chlorinated **16b–f** showed similar UV-Vis absorption as the unsubstituted parent compound **16a** with absorption maxima at 449 to 471 nm in solvents. In addition, their intense UV-Vis absorption and red-shifted behavior relative to quinoxaline (Fig. 3a, using **16a** as an example) suggested that two quinoxaline subunits were remarkably conjugated *via* the central CBD. However, this conclusion seemed to directly contradict the analysis of the bond lengths in single crystals (Fig. 3b). As all compounds showed the same molecular backbone in single crystals, compound **16a** was taken as a representative. For the four bonds in the CBD ring, half of them (C5a–C5b and C11a–C11b) are 1.5 Å long, which is even longer than the length of the single bond between two sp^2-hybridized carbon atoms in a typical non-conjugated system (1.47–1.48 Å). On the other hand, the length of the remaining two bonds (C5a–C5b and C11a–C11b, 1.44 Å) is larger than that of typical aromatic or alkenyl C=C double bonds but almost equal to the single bond between two sp^2-hybridized carbon atoms in a conjugated system (1.45–1.46 Å). Moreover, the length of the four C–N bonds (1.29–1.30 Å) around the central CBD is not only shorter than the other C–N

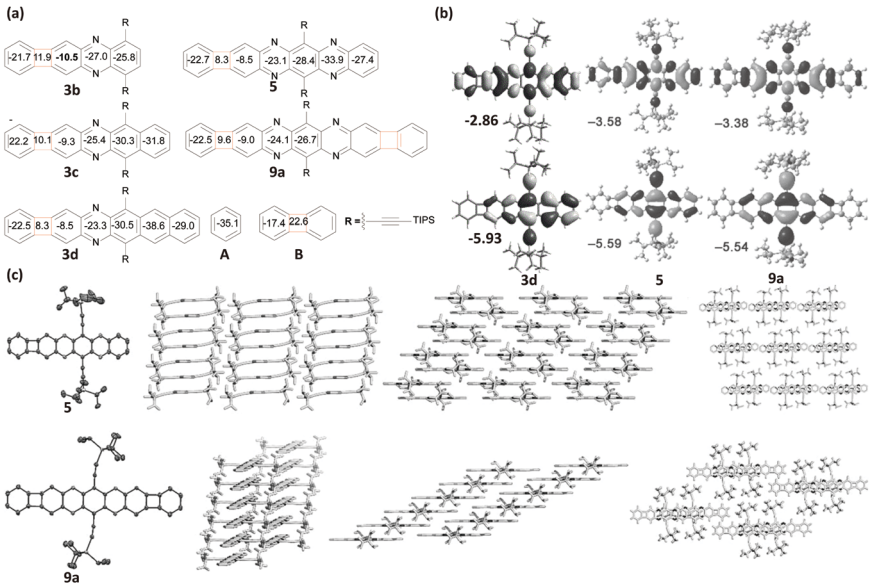

Fig. 2 (a) NICS $(1)_{\pi ZZ}$ calculations of compounds **3b-d**, **5** and **9a** compared to benzene **A** and biphenylene **B**. (b) Calculated frontier molecular orbital surfaces and LUMO (upper) and HOMO (bottom) energies (in eV) of **3d**, **5** and **9a** (from left to right). (c) X-ray crystal structure (left) and crystal packing (right) of **5** and **9a** from various angles. Adapted with permission from ref. 41 and 42. Copyright 2015 Wiley-VCH. Copyright 2016 Wiley-VCH.

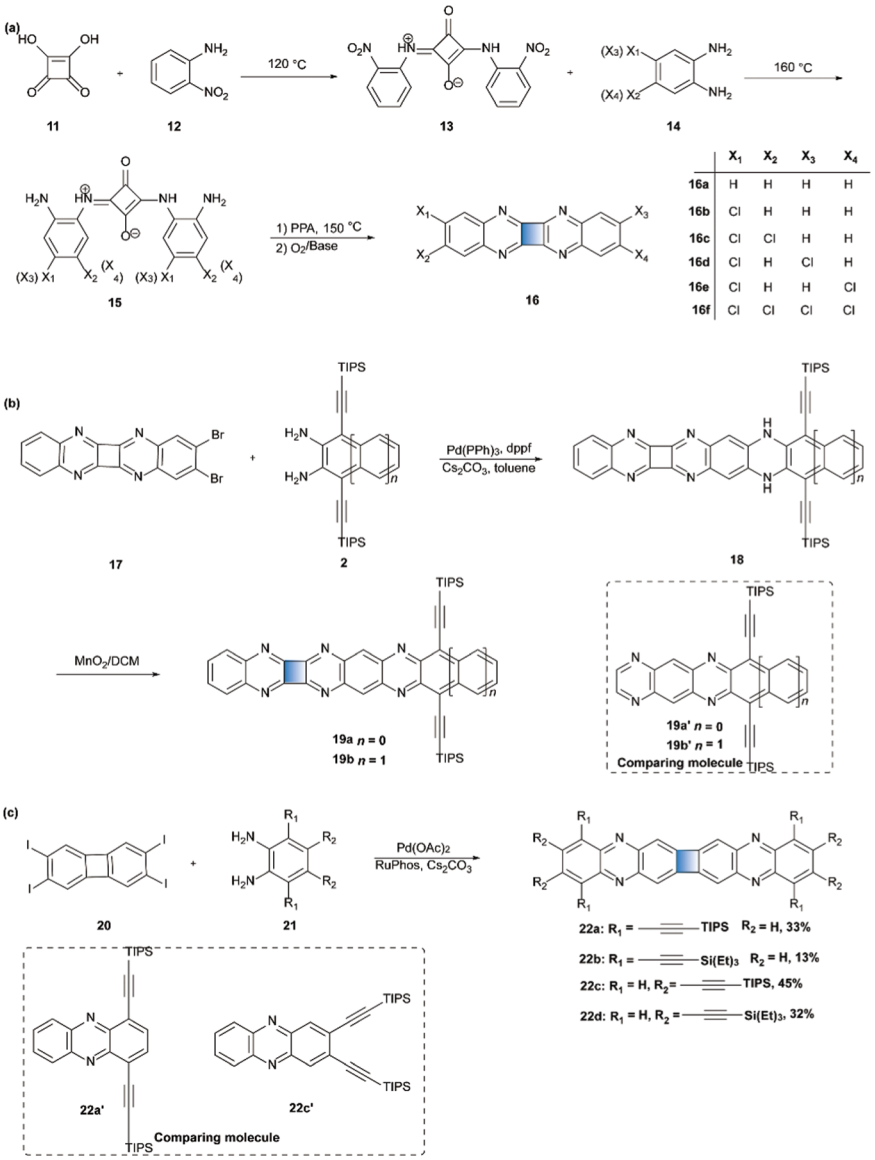

Scheme 2 Synthetic routes to compounds **16a–f**, **19a–b** and **22a–d**.

bonds in the structure, but also shorter than the typical C–N double in imines (1.35 Å). All these suggest that the conjugation between two quinoxaline subunits was very weak. Nevertheless, this contradiction could be explained by the special role of CBD units in the π-system, which often led to a weak conjugation in ground-state geometry in crystal structures but exhibited excited-state aromaticity in the UV-Vis absorption spectra.[20,52] The chlorine substituents did stabilize the HOMO and LUMO energy, and the estimated LUMO levels were lowered from −3.92 to −4.14 eV as the number of chlorine substituents increased from **16a** to **16f**. Their thin films were vacuum-deposited onto a high-*k* dielectric of 12-cyclohexyldodecylphosphonic acid (CDPA)-pre-treated aluminium oxide and titanium oxide (AlO_y/TiO_x) as semiconductors in OFETs, where **16e** and **16d**/**16e** exhibited a field-effect mobility of 0.23 ± 0.07 and 0.11 ± 0.05 $cm^2\ V^{-1}\ s^{-1}$, with the best performance up to 0.42, and 0.20 $cm^2\ V^{-1}\ s^{-1}$ under vacuum (Fig. 3c, Table 1), respectively. However, **16a-c** and **16f** were insulated, probably due to the face-on orientation or the morphology of isolated crystallites in the thin films.

The Pd-catalyzed aryl amination is an efficient method to build up pyrazine units in azaacenes. Considering that higher N-heteroacenes can principally feature more extensive electron delocalization and stronger interaction between π-planes in the solid states, this improves the n-type semiconducting performance in devices. Yang *et al.* synthesized two large π-conjugated systems through Pd-catalyzed coupling reactions (Scheme 2b).[43] They firstly prepared the *o*-brominated intermediate **17** by modifying the synthetic route of **16**, which reacted with phenylenediamine derivatives **2** in the presence of $Pd(PPh)_3$ and 1,1′-bis(diphenylphosphino)ferrocene (dppf) to afford dihydro form **18a**, partially with or without final compounds **19**, and treating the mixture or dihydro form intermediates with MnO_2 yielded the final compounds **19** in overall yields of 26–35% after a routine separation. Despite the

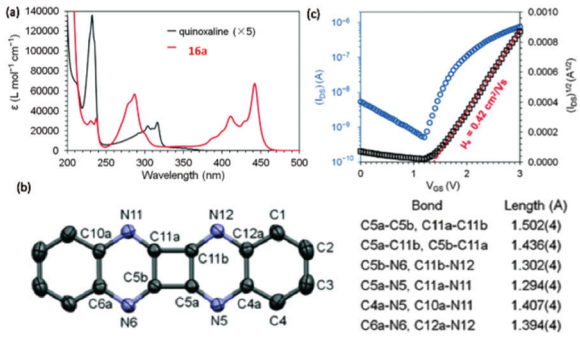

Fig. 3 (a) UV-Vis spectra for 0.01 mM solutions of **16a** in hexane/CH_2Cl_2 (99 : 1, v/v) and quinoxaline in hexane. (b) Crystal structure of **16a** with highlighted bond lengths. (c) Drain current (IDS) *versus* gate voltage (VGS) with a drain voltage (VDS) at 50 V for an OTFT of **16e** with an active channel of W = 1 mm and L = 50 mm as measured under vacuum. Reproduced with permission from ref. 51. Copyright 2015, Royal Society of Chemistry.

extended backbone, they displayed a very similar trend in properties as compounds **16**. Furthermore, the thin films of **19b** had a field-effect mobility of 0.015 ± 0.004 $cm^2\ V^{-1}\ s^{-1}$ in air, which was 10 times higher than that of **19a**. In contrast, the comparing compound **19a′** was an insulator and the field-effect mobility of **19b′** was only (4.1 ± 2.0) × 10^{-3} $cm^2\ V^{-1}\ s^{-1}$ in air. Following a similar approach, in 2018, the same group reported four symmetrical cyclobuta[1,2-*b*:3,4-*b′*]diphenazine (CBDPs) **22a–d** attaching four silylethynyl substitutions on different positions of the terminal rings to understand the effect of the substitution groups at the periphery and the role of the four-membered bridge in π-conjugation (Scheme 2c).[20] As expected, properly adjusting the position of silylethynyl substituting groups provided interesting optical and electronic properties. Only **22c** showed strong green fluorescence in CH_2Cl_2 solvent when excited at 513 nm, and the other materials including two comparison compounds exhibited negligible fluorescence. The varied substitutions gave apparent deviation from the FMOs energy levels, and the estimated LUMO levels based on the first reduction potentials for **22a–d** were −3.89 eV, −3.95 eV, −3.57 eV, and −3.62 eV, respectively. The dip-coated films of **22b** and **22c** consisting of crystalline ribbons and fibers were fabricated as n-type semiconductors into OFETs. Compound **22b** showed n-type semiconductor behavior with a field-effect mobility of 0.13 ± 0.05 $cm^2\ V^{-1}\ s^{-1}$ and the highest value of 0.3 $cm^2\ V^{-1}\ s^{-1}$ in vacuum, while the reference compounds **22a′** and **22c′** showed very poor performance due to their high LUMO energy level, the weak π-overlap in the solid states, and the limited stability of crystalline fibers.

Another apparent advantage of using CBD as the bridge to extend the azaacenes is the maintainability of the linear shape of the skeleton. To investigate the impact of different fusion patterns on the aromaticity of azaacenes, in 2018, the Xia group developed a class of linear, bent and angular-shaped CBD-containing azaacene regioisomers *via* their previously reported CANAL method.[23] As shown in Scheme 3, two linear CBD-containing azaacenes **25a–b** were furnished by CANAL between brominated phenazines and oxanorbornenes (*o*NBE) in the solvent of 1,4-dioxane at 150 °C, following an aromatization with strong acid. The overall two-step yield was as high as 50%. Moreover, the installation of dixylyl groups in compound **25b** ensured its solubility. Also, other bent and angular regioisomers **25c–d** and **25e** could be easily synthesized under similar conditions by adjusting the number and position of the brominated substitutions on the starting materials. As expected, the shape of the backbone significantly influenced the properties of the resultant materials. Compound **25b** showed much better stability than these bent or angular isomers and could persist for more than 10 days of light irradiation under ambient conditions without decomposition. Moreover, the as-obtained regioisomers displayed distinct features in absorption and fluorescence emission (Fig. 4a). The linear isomer **25b** exhibited strong absorption with λ_{max} = 503 nm and λ_{onset} = 523 nm, while the bent and angular isomers **25d** and **25e** showed broad absorption with a remarkable bathochromic shift due to the symmetry-forbidden HOMO–LUMO transition. Interestingly, only compound **25b**

Table 1 Summary of the physicochemical properties and performance

Compound	Abs_{max} (nm)	Abs_{edge} (nm)	Em_{max} [nm]	E_1^{red} [V]	HOMO [eV]	LUMO [eV]	Gap [eV]	Behavior	Ref.
16e	—	475	—	−1.06	−4.04	−6.65	2.61	Mobility in OTFTs: μ_e = 0.42 $cm^2\ V^{-1}\ s^{-1}$	51
19a	570	—	—	−0.77	−4.15[c]	−4.33[b]	2.11[a]	Mobility in OTFTs: μ_e = (1.5 ± 0.7) × 10^{-3} $cm^2\ V^{-1}\ s^{-1}$	43
19b	685	—	—	−0.68	−4.16[c]	−4.22[b]	1.7[a]	Mobility in OTFTs: 0.015 ± 0.004 $cm^2\ V^{-1}\ s^{-1}$	43
22c	513	—	527	−1.15	−6.29[d]	−3.50[d]	—	Mobility in OTFTs: 0.13 ± 0.05 $cm^2\ V^{-1}\ s^{-1}$	20
27bc	643	584	715	−1.04	−5.58	−3.76	1.82	Ambipolar organic semiconductors: μ_h = 2.77 × 10^{-4} $cm^2\ V^{-1}\ s^{-1}$ μ_e = 2.81 × 10^{-4} $cm^2\ V^{-1}\ s^{-1}$	53
32b	348, 366	—	348, 366	—	−5.33[c]	−2.03[b]	—	EQEs in PHOLEDs: 21.4%	54
36d	642	667	651	−0.83	−5.99[c]	−4.15[b]	1.84[a]	PCE in OPVs as acceptors: 1.6%	55
43e	550	—	—	−0.88	−6.23[d]	−3.98[d]	2.25	Mobility in transistors: μ_e = 0.037 $cm^2\ V^{-1}\ s^{-1}$	56
45c	422	610	—	—	−5.74[c]	−3.71[b]	2.03	PCE in inverted PSCs: 10.26%	57
47b	487	—	497	−1.56	−5.60[d]	−2.86[d]	2.45[a]	Max. luminance in OLED: 6 kcd m^{-2}	58
51c	397	—	—	−1.90	−6.03	−3.78	2.25	Mobility in OTFTs: μ_e = 0.005 $cm^2\ V^{-1}\ S^{-1}$	59
65b	475, 504	—	533	−1.91	—	—	2.33	Mobility in OFETs: μ_h = 0.07 $cm^2\ V^{-1}\ S^{-1}$	60
67	233, 266, 379	—	—	−1.22	−5.34	−3.20	2.43[a]	ON2/ON1/OFF current ratios in memory device: $10^{6.3}/10^{4.3}$/1	61

[a] Optical bandgap estimated by its UV-vis spectrum. [b] Energy level calculated from cyclic voltammograms. [c] Energy level calculated from CV data and the optical bandgap. [d] DFT calculation value. PSCs: perovskite solar cells. PCE: power conversion efficiencies; EQEs: maximum external quantum efficiencies; PHOLEDs: phosphorescent organic light emitting diodes.

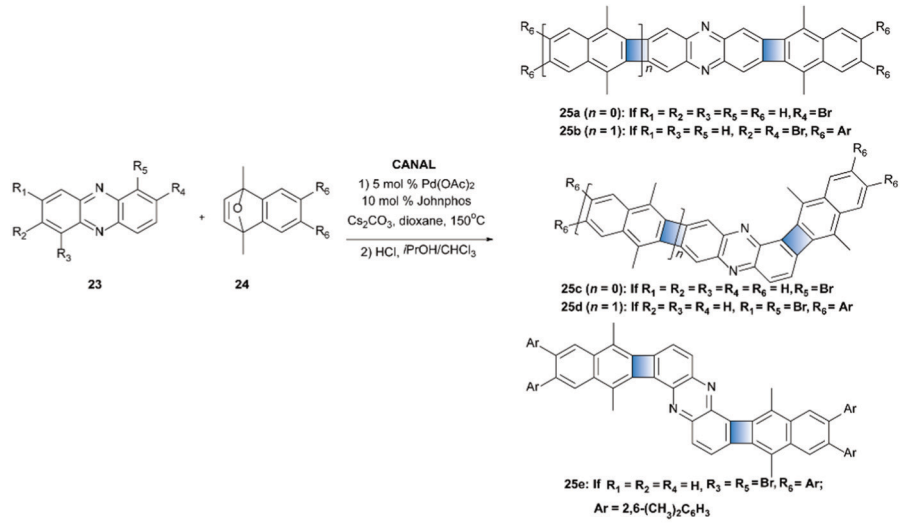

Scheme 3 Synthetic routes to compounds **25a–e**.

showed bright greenish-blue fluorescence with a quantum yield of 0.58. The estimated LUMO level based on cyclic voltammetry was decreased from −3.36 eV to −3.75 eV going from linear to angular isomers. NICS calculations (Fig. 4b) revealed that the enhanced anti-aromaticity as the backbone changed from linear to bent to angular shape resulting in the stabilized LUMO, the reduced bandgap, and the strongly quenched fluorescence.

3. Azaacenes bearing a five-membered ring

Embedding a five-membered ring into the molecular framework is an attractive way to fabricate novel structures with exciting properties such as aromatic, anti-aromatic, or diradical characters.[62,63] Additionally, incorporating multiple five-membered rings into the conjugation probably provides persistability against oxidative and photolytic degradation.[62,64] More importantly, their inclusion often improves the electron-accepting capabilities of these molecules,[65,66] especially when combined with the electron-withdrawing effect of the pyrazine ring in azaacenes.[59] As a result, their derivatives have been proven to be potential n-type or ambipolar organic semiconductors.[67] Basically, indene/fluorene, indenone, acenaphthylene and pyracylene (Fig. 5) are privileged motifs used to decorate the π-conjugation during the design of untypical N-heteroacenes.[68,69]

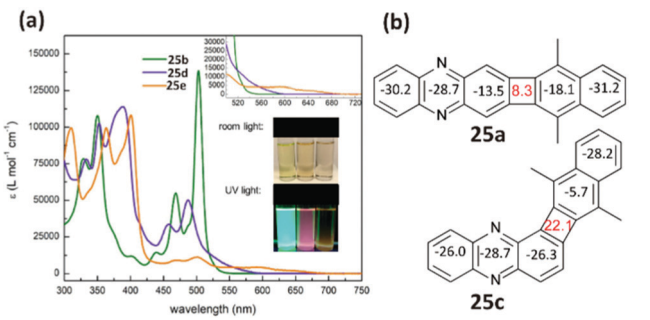

Fig. 4 (a) UV-Vis absorption spectra of **25b**, **25d**, and **25e** in $CHCl_3$. The inserted photographs are the dilute solutions of **25b**, **25d**, and **25e** (from left to right) under room light and 365 nm UV irradiation. (b) NICS $(1)_{\pi,ZZ}$ calculations on **25a** and **25c**. Reproduced with permission from ref. 26. Copyright 2018, American Chemical Society.

3.1. Indene/indanone-fused azaacenes

In 2016, the Bunz group[70] synthesized a series of N-heteroacenes (**27aa–ac**, **28aa**) containing a diazafluorene motif by condensation of different sizes of aromatic *o*-diamines with indanedione **26a** with yields ranging from 51% to 92% (Scheme 4a). The embedded five-membered ring seemed to have a minor influence on the general properties and showed the typical finger structure of azaacenes (Fig. 6a).

Currently, the precise control of energy levels is still quite challenging. Modifying the sp^3-hybridized carbon of a five-membered ring can offer very novel structures with interesting characters. For example, introducing the electron-withdrawing carbonyl group on the protruded carbon atom of diazaindenone can not only enhance the electron accepting ability,[66,71,72] but also restore the whole conjugated character of resultant azaacenes. In 2019, the Gao group[53] synthesized the indanone-fused azaacenes **27ba–bc** and **28ba** with different end-capped

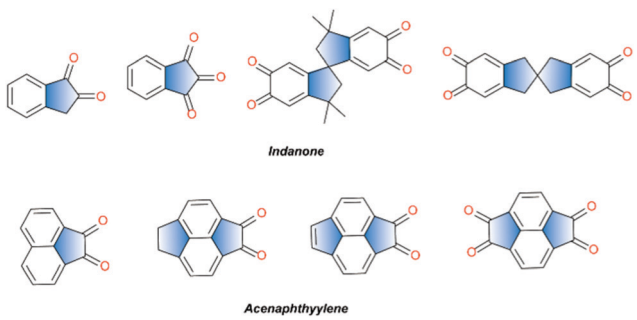

Fig. 5 Basic building blocks for constructing azaacenes bearing a five-membered ring.

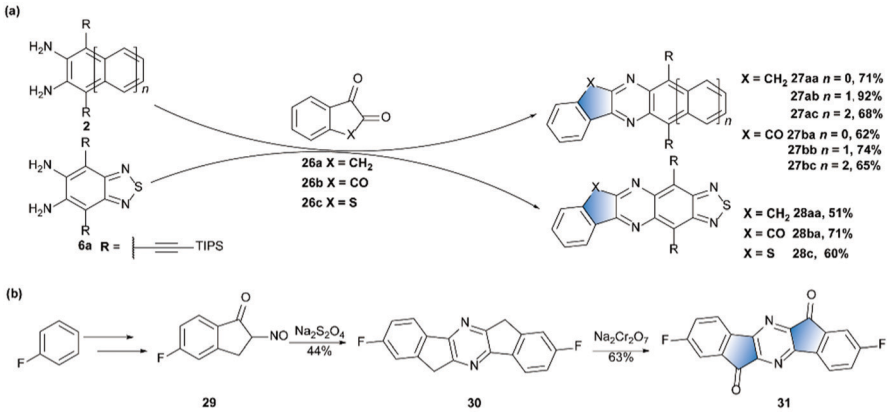

Scheme 4 Synthetic routes to compounds **27aa–ac**, **27ba–bc**, **28aa**, **28ba**, **28c** and **31**.

groups *via* the one-step condensation reactions between aromatic diamines and trione derivative **26b** in AcOH under 100 °C (Scheme 4a). In addition, in order to understand the impact of different fused units, **28c** fusing with a thienyl unit was also prepared in a similar manner. All compounds exhibited two reversible reduction waves with a slight increase of the first reduction waves in cyclic voltammetry as the size of the acene unit increased, and the values were also more positive relative to the corresponding non-carbonyl group-decorated species **27aa–ac** and **28aa**,[70,73] demonstrating their better electron accepting abilities (Fig. 6b and c). Significant bathochromic shifts were observed in UV/Vis and emission spectra as the acene backbones were enlarged from **27ba** to **27bc** (Fig. 6d). On the contrary, remarkable redshifts were observed compared with **27aa–ac**, corroborating the role of the attached carbonyl group in tuning the electronic delocalization, which was also in accord with the results of DFT calculations. For comparison, **27bc** and **28ba** were used to investigate their electron and hole mobilities *via* a space-charge-limited current (SCLC) method. As a result, **27bc** and **28ba** displayed balanced hole and electron transport characteristics, and the hole and electron mobilities for **27bc** were $\mu_h = 2.77 \times 10^{-4}$ cm^2 V^{-1} s^{-1} and $\mu_e = 2.81 \times 10^{-4}$ cm^2 V^{-1} s^{-1}, respectively. Yamashita's group[74] synthesized a series of indenofluorenediones to investigate their FET performance. In order to further increase the electron affinity, diindenopyrazinedione and its difluoride derivative **31** were also prepared *via* a five-step protocol using commercially available fluorobenzene as the starting materials (Scheme 4b),[74] and the critical pyrazine ring was formed by the self-condensation of 2-nitrosoindan-1-one **29**. Compared to the non-aza-substituted equivalent **31′**, incorporating nitrogen atoms led to a remarkable decrease in reduction potentials. The first and second reduction potentials for **31** and **31′** were −0.7 *vs.* −1.02 eV, and −1.32 *vs.* −1.52 eV, respectively, substantiating the N-doping strategy as an effective way to lower the LUMO levels. Single crystals showed that both compounds were planar, and **31′** adopted a face-to-face π-stacking with an interplanar distance of 3.30 Å. On the other hand, **31** displayed polymorphism with two different colored (red and black) single crystals because of the different degrees of overlapping (Fig. 6e). The black crystalline **31** and its non-fluorine derivative,[75] as well as **31′**, were fabricated on the hexamethyldisilazane (HMDS) treated SiO_2/Si substrates in a bottom contact geometry. As expected, all of them showed n-type FET behaviors despite the relatively low performances. The electron mobility of **31′** was 0.17 cm^2 V^{-1} s^{-1}, which was two orders of magnitude higher than **31** and its non-fluorine derivative. However, when fabricated in top contact geometry, the results were totally overturned. The performance for **31** was dramatically improved with a field-effect mobility of 0.17 cm^2 V^{-1} s^{-1} and on/off ratio of 10^7, while the value of **31′** was decreased to 6.6×10^{-2} cm^2 V^{-1} s^{-1} (on/off ratio: $\sim 10^4$) due to its rough surface leading to the poor contact between the active layer and the electrodes.

Besides the role in tuning energy levels,[71,72,76] another advantage of attaching carbonyl groups in the system is to facilitate the post-functionalization of materials. Liu *et al.*[54] spiraled the carbon by reacting diazafluorenone derivatives with lithiated triphenylamine to yield three novel spirocycles, 10-phenyl-10*H*-spiro[acridine-9,9′-indeno[1,2-*b*]pyrazine] (**SAIP**, **32a**), 10-phenyl-10*H*-spiro[acridine-9,11′-indeno[1,2-*b*]quinoxaline] (**SAIQ**, **32b**) and 10-phenyl-10*H*-spiro[acridine-9,13′-benzo[*g*]indeno[1,2-*b*]quinoxaline] (**SABIQ**, **32c**) (Scheme 5). This novel design produced very different properties relative to those typical N-heteroacenes. Three spiral materials displayed excellent thermal behaviors with decomposition temperatures as high as ∼400 °C due to the rigid and bulky spiro-structures. Their triplet energies (E_Ts) were calculated to be 2.71 eV for **SAIP**, 2.47eV for **SAIQ**, and 2.38 eV for **SABIQ** based on the first emission peaks in the well-defined Phos spectra, which were lower than their non-aza-substituting analogues[77] because of the electron-withdrawing effect of the pyrazine unit. Three compounds were fabricated as host materials in blue, green and red phosphorescent OLEDs (PHOLEDs) to explore their electroluminescence (EL) properties. Due to the high E_Ts and good thermal stability, **SAIP** and **SAIQ** based green and red devices exhibited better performances with maximum CE/PE/EQE values of 62.5 cd A^{-1}/81.5 lm W^{-1}/17.8% and 63.0 cd A^{-1}/82.3 lm W^{-1}/17.9%, respectively. Moreover, their charge transport properties were also investigated by fabricating them as hole-only and electron-only devices. **SAIP** and **SAIQ** displayed the bipolar transport characters with the estimated hole- and electron-mobility of

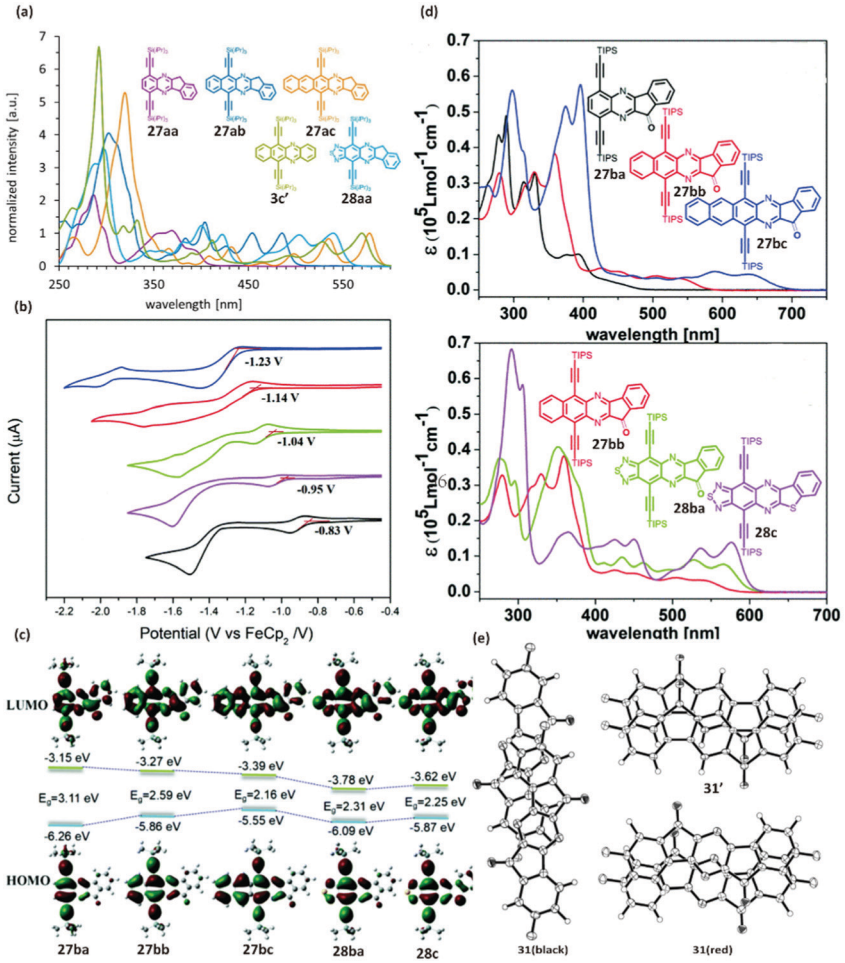

Fig. 6 (a) Normalized (lowest-energy maximum) absorption spectra of **27aa–27ac**, **28aa** and **3c**′ in *n*-hexane. (b) CV of **27ba–27bc**, **27bb**, **28ba**, and **28c** in CH_2Cl_2 and 0.1 M Bu_4NPF_6 on a Pt electrode at a scan rate of 50 mV s^{-1} *vs.* Ag/AgCl wire. (c and d) Absorption spectra and frontier molecular orbital diagram of **27ba–27bc** (upper) and **27bb**, **28ba**, and **28c** (bottom) in CH_2Cl_2. (e) Packing structures of **31** (black, left; red, right, bottom) and **31**′ (right, upper) in single crystals. (a) was reproduced with permission from ref. 70. Copyright 2016, American Chemical Society. (b, c, and d) were reproduced with permission from ref. 53. Copyright 2019, Royal Society of Chemistry. (e) was reproduced with permission from ref. 74. Copyright 2008, American Chemical Society.

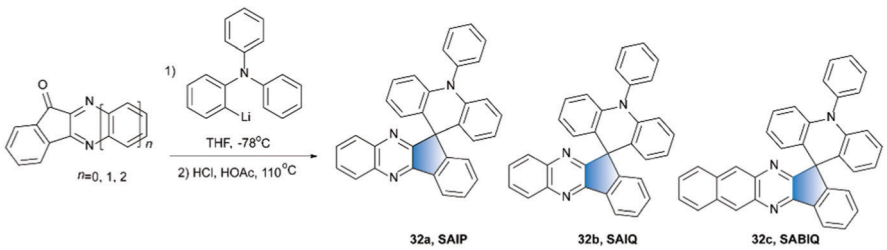

Scheme 5 Synthetic routes to compounds **32a–c**.

$\mu_{SAIP,h} = 6.2 \times 10^{-5}$ cm V^{-1} s^{-1}, $\mu_{SAIP,e} = 1.3 \times 10^{-7}$ cm V^{-1} s^{-1}; $\mu_{SAIQ,h} = 5.7 \times 10^{-5}$ cm V^{-1} s^{-1}, and $\mu_{SAIQ,e} = 3.2 \times 10^{-7}$ cm V^{-1} s^{-1}, respectively. Despite the mediocre performances, these studies opened new horizons for potential applications of azaacenes.

The strong tendency to crystallize hampers the applications of azaacenes in modern bulk-heterojunction organic photovoltaic devices (OPVs). Oligomerization is a useful approach to alleviate aggregation and modulate morphology in bulk or mixtures, thus improving the photovoltaic performance. The Bunz group disclosed a series of azaacene dimers (**36a–c**, **36e**) spiro-bridged through two five-membered rings. As shown in Scheme 6, they first prepared the key building block **33** by

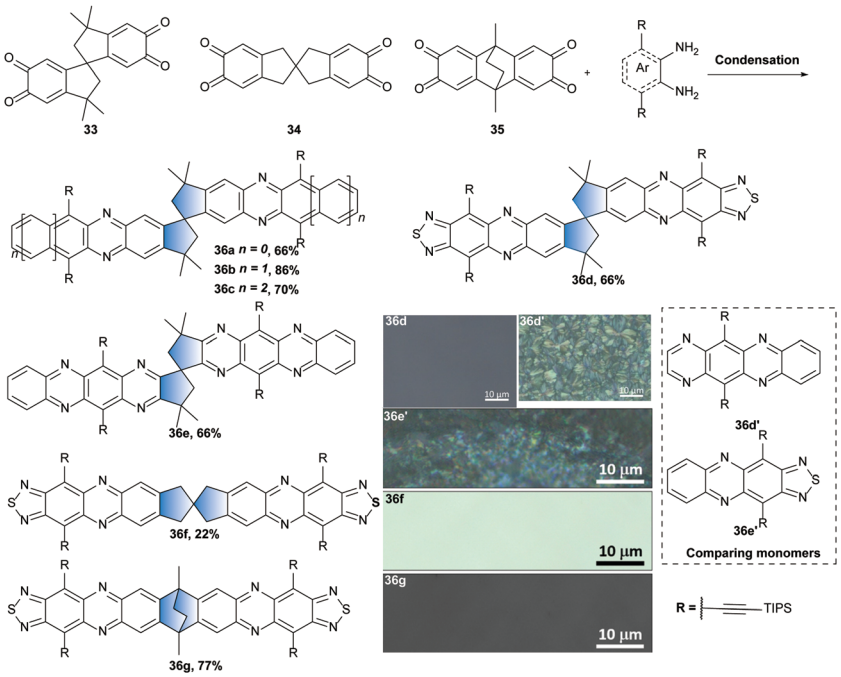

Scheme 6 Synthetic routes to azaacene dimers **36a–g** (inserted photographs are microscopic images of the spin-coated thin films of **36d**, **36f**, **36g** and **36d′**, **36e′**). Reproduced with permission from ref. 55 and 78. Copyright 2019, John Wiley and Sons. Copyright 2021, Royal Society of Chemistry.

$NaIO_4$ oxidation of the corresponding tetraol precursor. Its high reactivity but good stability at ambient conditions facilitated the condensation reactions with different diamines, thereby producing the spiro-connected targets with high yields.[55,78] In addition, due to the outstanding performance of thiadiazol derivatives as active elements in organic conductors and solar cells,[79–82] the analogues of phenazinothiadiazole dimers (**36d**, **36f**) were prepared and studied similarly. It is worth noting that one dimer (**36g**) bridged by a nonaromatic six-membered ring was also prepared to investigate the impact of the linker on crystallinity. The dimerization almost had no effect on the UV/Vis absorption in solution compared with the corresponding monomers **36′**, and the narrowed and well-resolved UV/Vis spectra in spun-cast thin films suggest that they have fewer intermolecular interactions and less π-stacking and thus formed amorphous films, which was supported by polarizing light microscopy (inserted photographs in Scheme 6). In contrast, the companion monomers were often crystalline. All compounds were investigated as electron acceptors in organic bulk heterojunction (BHJ) solar cells by mixing with the donor polymer (**PTB7**). The rising features below 500 nm from the external quantum efficiency spectra indicated their contribution to the photocurrent generation as acceptors since only negligible absorption came from the donor **PTB7** in this spectral range. Among them, **36d** displayed a maximum conversion efficiency of 1.62% without extensive optimization.

Recently, Wang *et al.*[63] reported a conjugated diradical 10,12-diaryldiindeno[1,2-*b*:2′,1′-e]pyrazine (**m-DIP2**) by simply altering the carbonyl groups with two stabilizing 9-anthryl groups through a two-step reaction (Scheme 7a). Meanwhile, the control molecule of 10,12-diaryldiindeno [1,2-*b*:1,2′-*e*] pyrazine (**p-DIP**) was also prepared for comparison. Surprisingly, ***m*-DIP2** presented a quite stable triplet ground state and could persist for a long time with a half-life time of 22 days under ambient conditions, which was far more stable than the isomer of indeno-[1,2-*a*]fluorene,[62] and one of the slow decomposition compounds was **m-DIP-mono2**. UV-Vis-NIR absorption spectra showed that the diradical ***m*-DIP2** had a dramatically broadened near-infrared absorption band (up to 1200 nm) driven by the structurally radical character. However, the comparison compound ***p*-DIP** only displayed common absorption characteristics as indenofluorene-related structures. An electron paramagnetic resonance experiment is a useful way to detect the radical ground state nature of molecules. A sharp featureless peak in the continuous-wave electron paramagnetic resonance spectra (cw-EPR) demonstrates the open-shell triplet electronic structure of ***m*-DIP2** (Fig. 7a). According to the calculation, the spin density mainly delocalized within the *meta*-pyrazine motifs (Fig. 7b), and the calculated singlet–triplet gap (ΔE_{S-T}) of ***m*-DIP2** was 1.01 kcal mol^{-1}. In addition, nucleus-independent chemical shift (NICS)-*XY* scans were performed to explain the differences between their electronic structures. The results suggested that the central pyrazine ring in the closed-shell singlet ***p*-DIP** was a 4π electron system with anti-aromaticity, while it was a triplet state with 6π electrons in ***m*-DIP1** (simplified molecule of ***m*-DIP2** for calculation). The outer benzenoid rings exhibited significant aromaticity, suggesting ***m*-DIP1** to be a better representative upon Hückel-aromatic rules. Furthermore, a long spin lattice relaxation time (T_1) of 4.3 ms and quantum phase memory time (T_3) of 3.0 ms were observed in

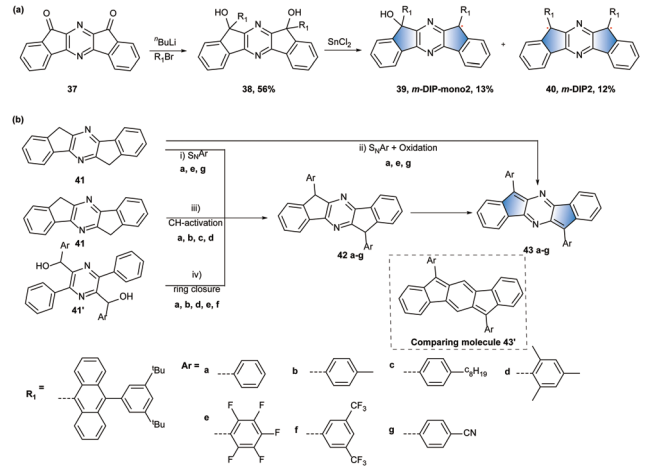

Scheme 7 Synthetic routes to compounds **40** and **43a–g**.

m-DIP2 solution, indicating its promising applications in organic spintronics. Later on, the Bunz group[56] did a similar work and successfully synthesized a group of diindenopyrazines **43a–g** through three different routes depending on the substitution groups (Scheme 7b). They found that the solubility, redox potentials, and optical properties could be modulated by the introduction of different functional aryl groups on the 6- and 12-positions. Particularly, the absorption of compounds **43d** and **43e** was the most blue-shifted compared to other compounds due to the larger degree of twisting of the aryl rings with respect to the diindenopyrazine (Fig. 7c), whereas all the compounds exhibited a red-shift in comparison with indenofluorene **43′** because of the favorable planar geometry and electronic effect of the pyrazine ring. Furthermore, their HOMO and LUMO levels were stabilized by the electron-withdrawing pyrazine unit, and the electron affinity of **43e** was surprisingly decreased to −4 eV. As a representative, the drop-cast crystalline thin film of **43e** was used in transistors and displayed an average mobility of 0.022 $cm^2 V^{-1} s^{-1}$ with a top mobility of μ_{max} = 0.037 $cm^2 V^{-1} s^{-1}$. It is worth noting that this un-optimized result was an order of magnitude higher than that of **43′**.[63]

3.2. Acenaphthylene and its analogue fused azaacenes

Due to the structural resemblance to fullerene and its remarkable optoelectronic properties,[83,84] pyracylene has been found to be an intriguing subunit during the design of novel functional materials for organic semiconductors and ferromagnets.[85,86] From this perspective, Zhang and co-workers attempted to introduce a pyracylene unit into the conjugation of azaacenes. They revealed three different-sized azaacenes containing a pyracylene motif, two of the symmetrical structures **45a** (**TBIDQ**)[87] and **45b** (**DQNDN**)[88] were synthesized directly through a one-step condensation reaction between 1,2,5,6-tetraketopyracene **44** and corresponding *o*-diamine derivatives under acidic conditions with around 70% yield (Scheme 8). For the unsymmetrical **45c** (**QCAPZ**),[57] the intermediate **46** was first produced by the mono-condensation of **44** with polycyclodiamine **4** in acetic acid solution, then the as-precipitated purple powder was directly reacted with *o*-phenylenediamine in pyridine to afford the target in 82% yield. The attached triisopropylsilyl (TIPS) groups on the backbone were used to tune the molecular packing and improve the solubility. Among them, **DQNDN** was an ambipolar material according to Mott–Schottky measurements. The nanostructured **DQNDN** was fabricated by slowly dropping ethanol into its trifluoroacetic acid solution under vigorously stirring (Fig. 8a and b). The whole absorption of the nanostructured **DQNDN** film in the visible

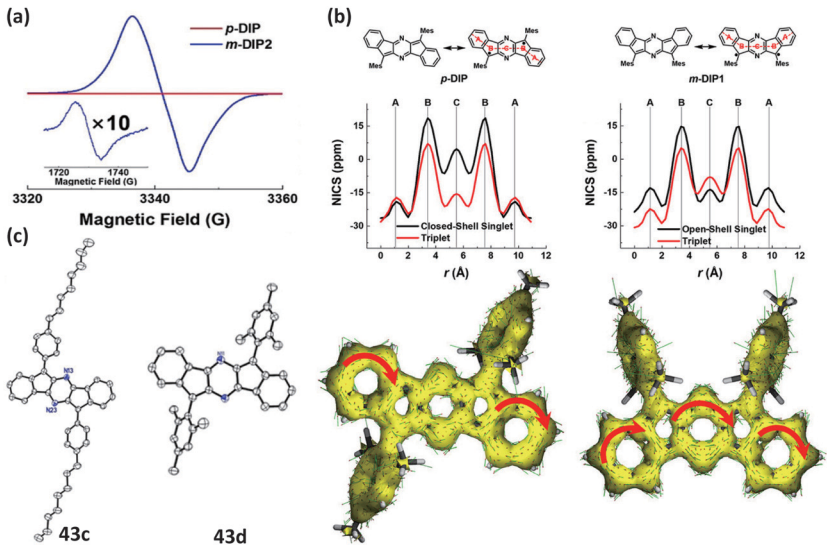

Fig. 7 (a) EPR spectra of **m-DIP2** and **p-DIP** in the $\Delta m_s = \pm 1$ region (insert: the EPR signal of **m-DIP2** in the $\Delta m_s = \pm 2$ region). (b) Theoretical assessment of **m-DIP1** and **p-DIP**. (c) Single crystal structure for **43c** and **43d**. (a and b) reproduced with permission from ref. 63. Copyright 2021, John Wiley and Sons. (c) was reproduced with permission from ref. 56. Copyright 2021, John Wiley and Sons.

spectrum region suggested its promising application in photoelectrodes in photoelectrochemical cells (PECs). When it was tested as a photocathode in a PEC (Fig. 8c), it exhibited high stability and efficiency with the largest current density of 0.13 mA cm^2 at 0.13 V *versus* RHE (Fig. 8d). **QCAPZ** was used as an electron-transport layer (ETL) for inverted perovskite solar cells. The strong absorption from 300 nm to 500 nm and the shrunken emission around 775 nm in the bilayer perovskite/**QCAPZ** thin film demonstrated that the electrons could transfer from the perovskite to **QCAPZ** effectively at the perovskite/**QCAPZ** interface (Fig. 8e and f). As expected, the power conversion efficiency (PCE) was as high as 10.26% with a current density of 16.55 mA cm^{-2} and an open-circuit voltage of 0.86 V when used as an ETL in inverted perovskite solar cells (Fig. 8g and h). Despite the relatively low current density value resulting from the mismatch of energy levels between perovskite and **QCAPZ** (conductive band of −3.9 eV *vs.* LUMO level of −3.71 eV), the fill factor was up to 72.1%, which was competitive with those of traditional fullerene PCBM-based perovskite solar cells. Adopting a similar strategy, a large amount of (acena)(dihydro)phthylene-decorated molecules (**47a–c**, **48a–e** and **49a–c**) were prepared by the Bunz group to explore their structure–property relationships (Fig. 9).[58] Their emissions in the solid states were dramatically changed along with the varied saturability of the terminally annulated five-membered ring due to the changing of excited singlet states in the molecules, and the crystalline powders displayed distinct colors in solid states under ultraviolet irradiation.[89] Therefore, their applications as emitters in organic light-emitting diodes have been investigated. As a result, green-emitting acenaphthylene **47b** showed a remarkably higher luminance (5.8×10^3 cd m^{-2}), maximum efficiency (2.88 cd A^{-1}) and efficacy (0.83 lm W^{-1}) than the remaining materials. Additionally, more congeners were also synthesized by the Xiao group (**PyAP**, **50**)[90] and Chi group (**BAPQs**, **51a–c**)[59] in a similar manner. Interestingly, a distinct colour change was observed in the UV/Vis absorption and fluorescence spectra of **PyAP** after the addition of strong protic acid, suggesting its potential application as "naked-eye" probes for protons.

Very recently, the Krische group[25] synthesized a class of highly soluble N-doped rubicenes through their previously reported strategy of ruthenium-catalyzed butadiene-mediated benzannulation. Initially, chemoselective condensation of the critical tetraketone **52** with various 1,2-diamines enabled monocondensation products **53a–d** in good yields (Scheme 9a). However, an additional step of aromatization with 2,3-dichloro-5,6-dicyano-1,4-benzoquinone (DDQ) was needed when saturated vicinal diamines were employed (**53d**). After that, the butadiene benzannulation of N-doped diketones **53a–d** was conducted to form the initial cycloadducts, which readily underwent *p*-TsOH-catalyzed dehydrative aromatization to provide N-doped rubicenes **55a–d** in moderate to good yields. Alternatively, as illustrated in Scheme 9b, the tetraazarubicene **55e** could also be effectively achieved *via* double condensation between tetraketone **52** and 1,2-diaminocyclohexane with comparable yield. Spectroscopic and theoretical research indicated electronic states of the rubicene core was scarcely impacted by the end-capping substituents, whereas the solid-state structures can be varied from a typical herringbone packing motif to a face-to-face arrangement in response to outer π-systems.

4. Macrocycle bridged azaacenes

Reports concerning azaacenes containing macrocycles (≥7-membered ring) are rare, presumably due to the limited synthetic strategies and uncertain properties in materials. On the other hand, introducing conjugated macrocycles into π-backbone of azaacenes is of significant fundamental interest. For example, inclusion of different-sized macrocycles can give the intriguing size-dependent electronic and optical properties. Moreover, the inherent non-planar character of a conjugated macrocycle often yields negative curvature, leading to a saddle shaped geometry for the resultant molecules.

In 2018, the Bunz group reported a family of dibenzosuberone-fused N-heteroacenes with negative curvature.[91] They first prepared a highly reactive trione **57** by oxidation of dibenzosuberone with SeO_2, which could react with different aromatic diamines or tetraamines to give mono- or bissuberones end-capped targets (**58a–g**) in moderate to high yields (Scheme 10a). Interestingly, according to the UV-Vis spectra, it is easy to find that each added dibenzosuberone exerts a similar impact on the electronic properties as half of the attached benzene ring. For example, the absorption maxima for symmetrical **58f** and

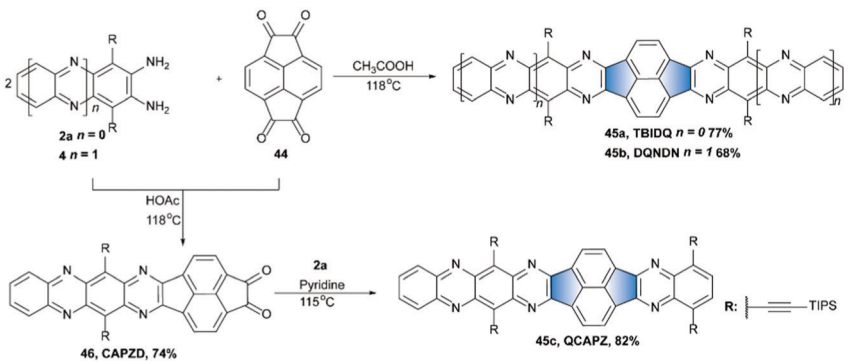

Scheme 8 Synthetic routes to compounds **45a–c**.

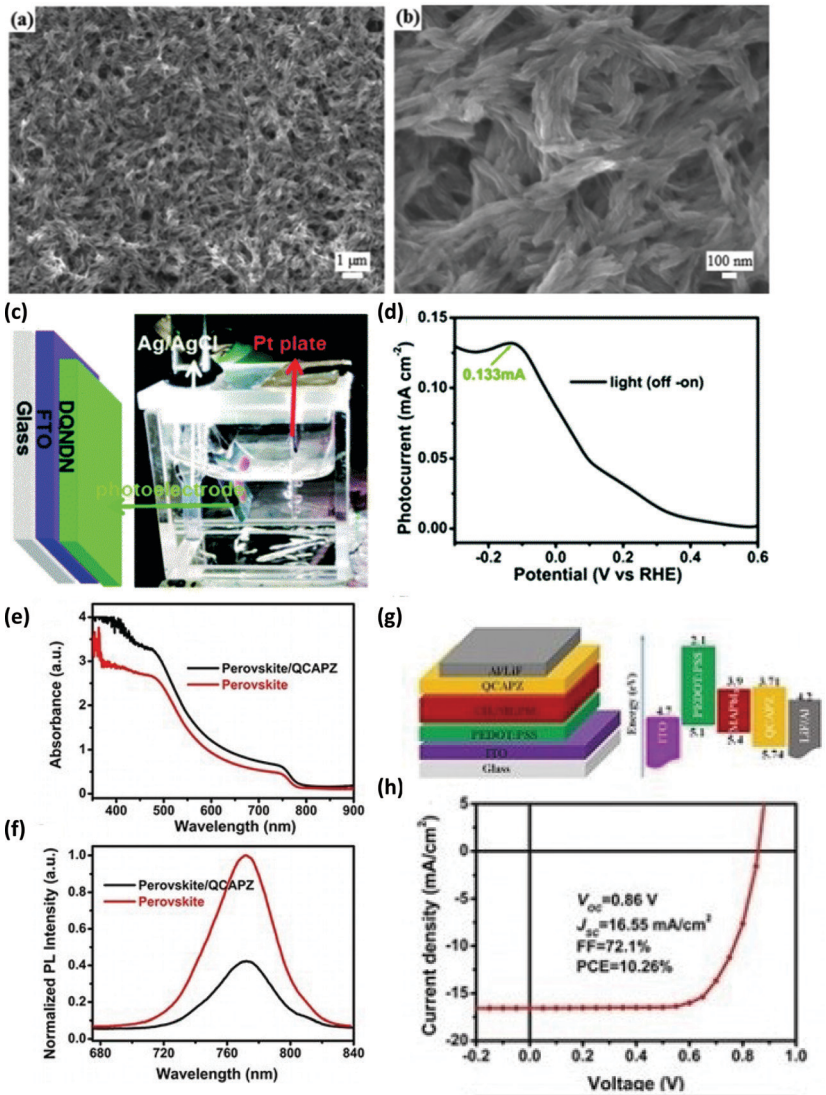

Fig. 8 SEM images of nanostructured **DQNDN** nanofibers. At (a) low resolution and (b) high resolution. (c) Device architecture and the PEC cell. (d) The corresponding current density–potential curve of **DQNDN**. (e) Absorption spectrum of perovskite and bilayer perovskite/**QCAPZ** thin films in the range of 350–900 nm. (f) Relative PL intensity of perovskite thin films with and without **QCAPZ**. (g) Device architecture and corresponding energy level diagram. (h) The device performance of a perovskite solar cell employing **QCAPZ** as the electron-transport layer. (a–d) were reproduced with permission from ref. 88. Copyright 2016, Royal Society of Chemistry. (e–h) were reproduced with permission from ref. 57. Copyright 2016, John Wiley and Sons.

58g are 544 and 731 nm, respectively, which are very close to the values of their corresponding hydrocarbon analogues.[92,93] All the as-prepared materials, except **58g**, exhibited bright fluorescence both in solution and in solid states (Fig. 10a). In particular, the quantum yield of solid-state **58b** was up to 0.23, which was much higher than the corresponding simple azaacene.[94] Their single crystals could be easily obtained based on their good solubility and stability in ambient conditions. As expected, all species displayed significant negative curvature in the solid state due to the inherent non-planar character of the seven-membered ring. **58c** and **58d** adopted a kinked brick wall motif with typical π-stacks (Fig. 10b, **58d** as an example), combined with their low band gap behaviors, making them promising materials for OFETs.

Moreover, the same group also reported several interesting azaacenes bearing an eight-membered ring.[95] The three different-sized cyclooctatetraene derivatives (**Di1-3**) could be synthesized by smooth coupling between tetrabromide **59** and the corresponding diamino-arenes in the presence of a highly loaded catalyst of PdRuPhos in yields ranging from 21 to 28% after oxidation with MnO_2 (Scheme 10b). It was noted that mono-coupled compound **Di2b** was one of the by-products during the synthesis of **Di1**. As a representative, **Di2** displayed a typical saddle-shaped structure in the solid state (Fig. 10c). The NICS scan of **Di2** presented a variation of the aromatic

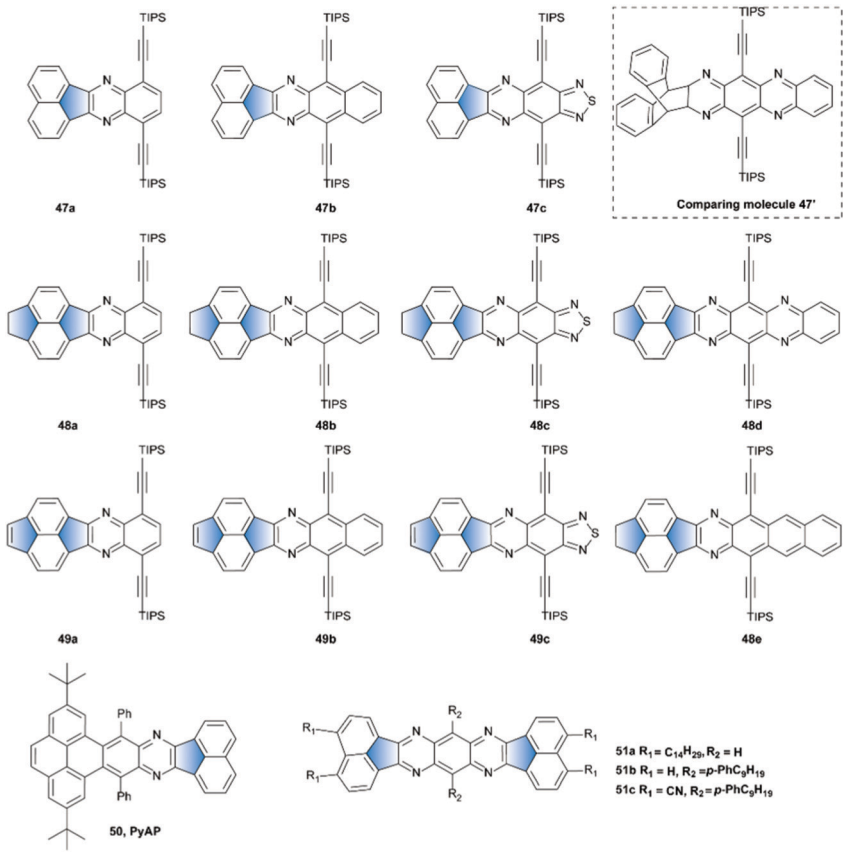

Fig. 9 Acenaphthylene and its analogue-decorated azaacenes.

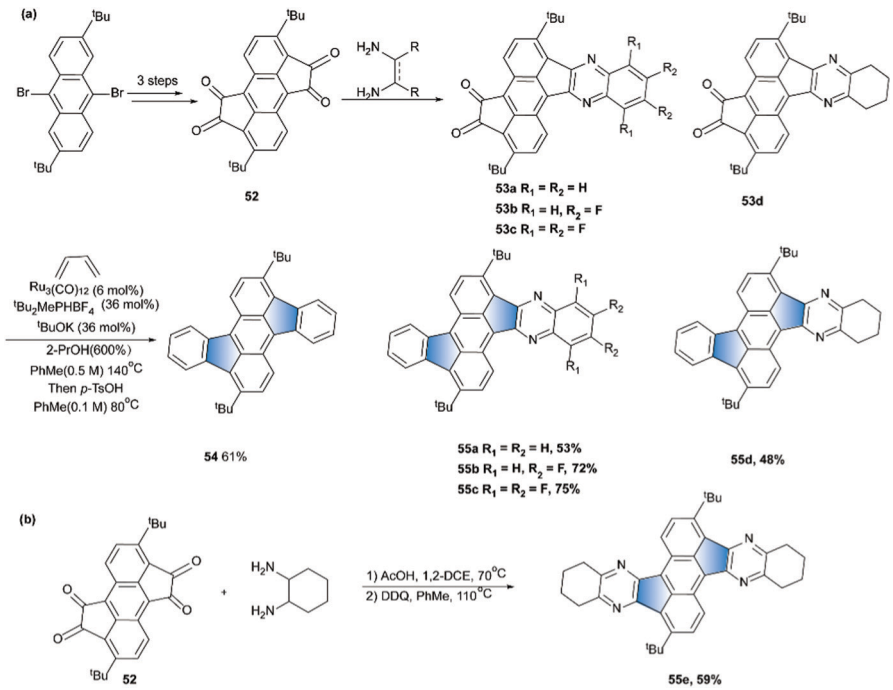

Scheme 9 Synthetic routes to compounds **53a–d**, and **55a–e**.

character along the scanned axis through the saddle-shaped cyclooctatetraene-ring (Fig. 10d). Obviously, the positive values in the saddle region corroborated the anti-aromatic property of the cyclooctatetraene unit. Very recently, Saito and coworkers[96]

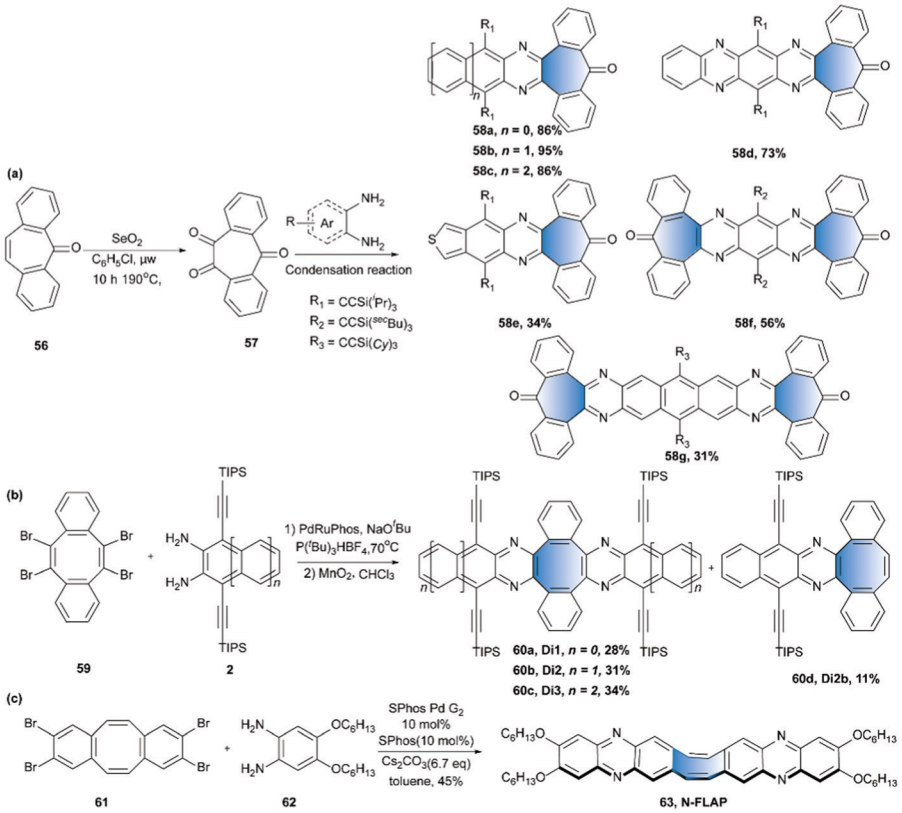

Scheme 10 Synthetic routes to compounds **58a–g**, **60a–c** and **63**.

developed a dual fluorescent flapping molecular probe (**N-FLAP**) to monitor the dynamic polymer free volume by single-molecule spectroscopy (Scheme 10c). The introduction of nitrogen atoms into the backbone not only alleviated undesired photoreactions, but also enabled efficient visible excitation, leading to a significant improvement in brightness (22 times) compared to the previously reported flapping anthracene analogue. When it was dispersed in a spin-coated polystyrene thin film to determine the polymer free volume, due to the presence of the bridging cyclooctatetraene ring, a bent-to-planar conformational change could take place in the lowest singlet excited state (S_1), and more importantly, it immediately went back to the most stable V-shaped structure in the singlet ground state (S_0), resulting in frequent jumps between short- and long-wavelength form in single molecular fluorescence spectra (Fig. 10e). As the dynamic planarization process requires certain free space, which can be driven by the segmental relaxation of surrounded polymers (Fig. 10f), the polymer-free volume was thus roughly determined according to the time intervals of the green fluorescence excitation and emission in a flapping molecular probe.

5. Azaacenes containing additional heterocycles

In addition to the above-mentioned strategies, end-capping or interspersing the extra heterocycles (S, N O, *etc.*) into the backbone of azaacenes is also a general way to tune the properties and construct very novel materials (Fig. 11).[97–99] For example, Jia *et al.* developed a donor–acceptor system integrating pyrene-based azaacene with tetrathiafulvalene (TTF) together (**64**). The enhanced oxidation potentials relative to TTF suggest the good electronic transporting ability between the donor and acceptor. Besides, N-containing heterocycles including carbazole,[60] imidazole,[100–102] indolizine,[103] *etc.*[65,68,104–106] are more popular decorating units for azaacenes. For example, Liao *et al.*[60] synthesized a series of stable and soluble carbazole-containing azaacenes (**65a-c**) *via* sample condensation reactions. The carbazole rings acted as donors while two pyrazine units were acceptors in one molecular skeleton. In particular, single-crystal transistor devices based on **65b** displayed p-type behavior with a hole mobility of 0.07 $cm^2\ V^{-1}\ s^{-1}$. Arnold and co-workers developed two imidazole-linked ladder-type polymers (**66a**, **b**) by condensation of tetraazahexacene-tetraamine with naphthalene-1,4,5,8-tetracarboxylic acid or pyromellitic anhydride.[107,108] These two azaacene-type polymers exhibited good thermal stability both in nitrogen and air atmospheres. Since 2013, Zhang and coworkers[61,109–112] have developed a series of novel O-bridged azaacenes and investigated their ternary memory behaviors in storage devices. The results of UV-Vis and CV suggested their smaller bandgaps compared with corresponding classic aza-bridged equivalents, indicating the destruction of conjugation by an O-bridge.[109] Especially, compound **67** exhibited excellent ternary memory behavior with high ON2/ON1/OFF current ratios

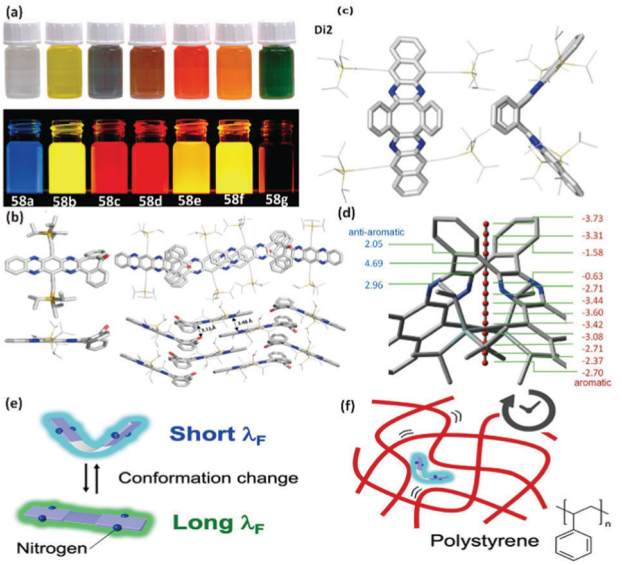

Fig. 10 (a) Pictures of **58a–g** (from left to right) under ambient light (top) and UV-light (bottom, $\lambda_{max,ex}$ = 365 nm). (b) Single crystal structures and packing of **58d**. (c) Different views of the single crystal structures of **Di2**. (d) Calculated structure and NICS values of **Di2** with ghost atoms along the scanned axis through the saddle-shaped cyclooctatetraene-ring. (e) Schematic of bent-to-planar conformational change. (f) Real-time analysis of polystyrene free volume using the **N-FLAP** dopant. λF: Fluorescence wavelength. (a and b) were reproduced with permission from ref. 91. Copyright 2020, American Chemical Society. (c and d) were reproduced with permission from ref. 95. Copyright 2018, John Wiley and Sons. (e and f) were reproduced with permission from ref. 96. Copyright 2021, American Chemical Society.

of $10^{6.3}/10^{4.3}/1$ and good stability for the three states. Kaafarani and coworkers synthesized a series of cation sensors by fus ing the pyrene–pyrazine system with different-sized crown ethers (**69a–d**).[113–115] These pyrene discotics responded to an array of alkali and alkaline-earth metals and the efficacy of interaction could be easily monitored through UV-Vis, fluorescence and nuclear magnetic resonance spectroscopies.

In all, diverse structures of heterocycles significantly enrich this sub-class of azaacenes. Concomitantly, the special properties of newly introduced heterocycles often induce very different behaviors from the typical azaacenes. Moreover, the properties of the resultant materials are sometimes even dominated by the additional heterocycles, which provides possibilities to get unexpected performances in devices. No doubt, their distinctive properties will continue to captivate new generations of researchers.

6. Conclusions

In this review, we summarized the synthetic routes, properties, and applications of one group of untypical azaacenes, and elaborated the roles of the inserted nonbenzenoid units in the system. Due to the long history, exciting features, and excellent performance as semiconductors, the existence of the well-defined (aza)acenes overshadowed the development of this subgroup of azaacenes bearing nonbenzenoid rings to some extent. Indeed, as they share the same subunit of pyrazine, their

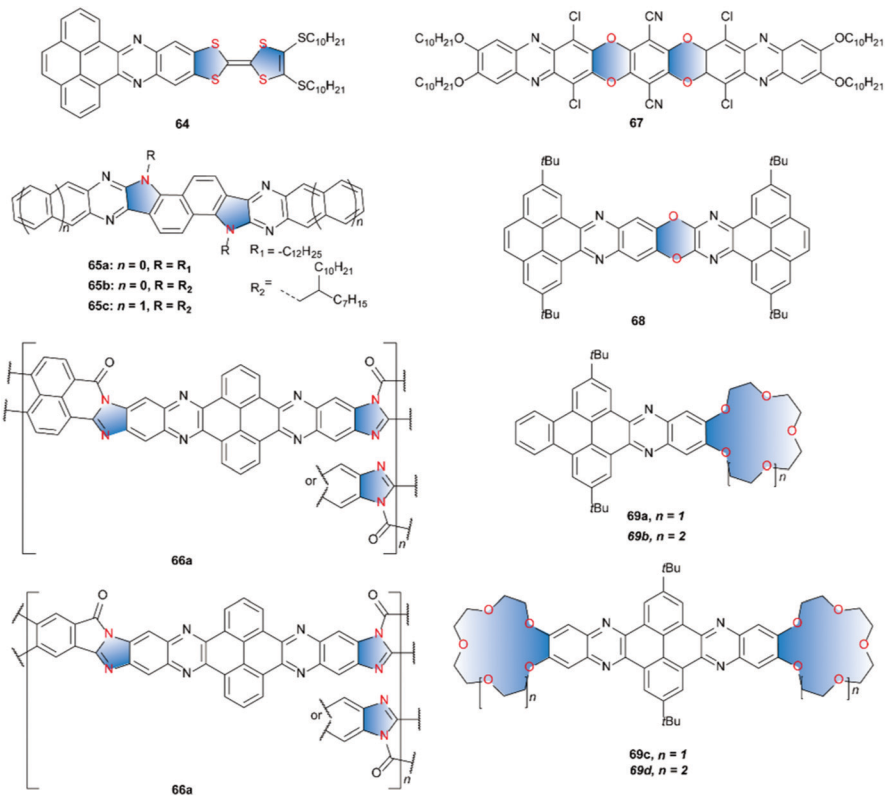

Fig. 11 Azaacenes containing the additional heterocycles.

synthetic strategies usually arise from the modification of classic approaches towards those well-defined azaacenes, while the modular synthetic approach of CANAL ensured the high efficiency to approach diverse CBD-containing azaacenes. Furthermore, the ruthenium-catalyzed butadiene-mediated benzannulation strategy allows fast and efficient access to five-membered ring annulated azaacenes with novel structures. Obviously, introducing these nonbenzenoid units into the π-conjugation of azaacenes not only diversifies this family of molecules but provides theoretical and practical significance. On one hand, their inclusion confers the stability of the resultant materials, thus offering the opportunities to explore their applications in organic devices. For example, an unoptimized performance with a PCE of 10.26% and a fill factor up to 72.1% was realized when using **QCAPZ** as an electron-transport layer in PSCs, and this fill factor could compete with those of fullerene PCBM-based perovskite solar cells. On the other hand, their inherent characters offer advantages in the investigation of structure-related applications. For example, the flapping molecular probe of **N-FLAP** succeeded in the direct and quantitative evaluation of polymer free volume depending on the rapid switching of the cyclooctatetraene ring between bent and planar conformations.

As mentioned in this review, many strategies such as chlorine substitution, thiadiazol fusing and dimerization have been attempted in order to improve the performance of the resulting materials in devices. There is no doubt that most of the disclosed device performances are still not satisfactory. Therefore, there is still great potential for investigation of many aspects. Future research efforts should first focus on developing powerful methods to approach the processable and stable molecules with novel skeletons, as well as to improve the performance in organic electronics. Besides, despite the investigation of traditional photoelectric and photophysical property-based devices such as OFETs, solar cells and OLEDs, emphasizing their inherent characters such as structural curvature effect, anti-aromatic and diradical properties and developing related applications may provide more exciting results. Along this direction, we believe that increasing scientific interest will be focused in this direction as a result of the property-based advantages over their classic congeners.

Conflicts of interest

There are no conflicts to declare.

Acknowledgements

QZ acknowledges the support of starting funds from the City University of Hong Kong.

Notes and references

1 J. E. Anthony, *Angew. Chem., Int. Ed.*, 2008, **47**, 452–483.
2 Q. Zhang and J. Li, *Synlett*, 2013, 686–696.
3 C. Tönshoff and H. F. Bettinger, *Chem. – Eur. J.*, 2020, **27**, 3193–3212.
4 J. Shi and C. W. Tang, *Appl. Phys. Lett.*, 2002, **80**, 3201–3203.
5 J. Takeya, M. Yamagishi, Y. Tominari, R. Hirahara, Y. Nakazawa, T. Nishikawa, T. Kawase, T. Shimoda and S. Ogawa, *Appl. Phys. Lett.*, 2007, **90**, 102120.
6 X. Shi and C. Chi, *Chem. Rec.*, 2016, **16**, 1690–1700.
7 J. Li, Y. Shen, J. Wan, X. Yu and Q. Zhang, *Eur. J. Org. Chem.*, 2018, 3375–3390.
8 Y. Wu, Y. Jin, J. Xu, Y. Lv and J. Yu, *Curr. Org. Chem.*, 2020, **24**, 885–899.
9 Q. Miao, *Adv. Mater.*, 2014, **26**, 5541–5549.
10 A. Sosorev, D. Dominskiy, I. Chernyshov and R. Efremov, *Int. J. Mol. Sci.*, 2020, **21**, 5654.
11 Z. Wang, P. Gu, G. Liu, H. Yao, Y. Wu, Y. Li, G. Rakesh, J. Zhu, H. Fu and Q. Zhang, *Chem. Commun.*, 2017, **53**, 7772–7775.
12 R. K. Dubey, M. Melle-Franco and A. Mateo-Alonso, *J. Am. Chem. Soc.*, 2021, **143**, 6593–6600.
13 P.-Y. Gu, Z. Wang, G. Liu, H. Yao, Z. Wang, Y. Li, J. Zhu, S. Li and Q. Zhang, *Chem. Mater.*, 2017, **29**, 4172–4175.
14 U. H. F. Bunz and J. U. Engelhart, *Chem. – Eur. J.*, 2016, **22**, 4680–4689.
15 A. H. Endres, M. Schaffroth, F. Paulus, H. Reiss, H. Wadepohl, F. Rominger, R. Krämer and U. H. F. Bunz, *J. Am. Chem. Soc.*, 2016, **138**, 1792–1795.
16 G. J. Richards, J. P. Hill, T. Mori and K. Ariga, *Org. Biomol. Chem.*, 2011, **9**, 5005–5017.
17 J. Li and Q. Zhang, *ACS Appl. Mater. Interfaces*, 2015, **7**, 28049–28062.
18 U. H. F. Bunz, *Acc. Chem. Res.*, 2015, **48**, 1676–1686.
19 M. Müller, L. Ahrens, V. Brosius, J. Freudenberg and U. H. F. Bunz, *J. Mater. Chem. C*, 2019, **7**, 14011–14034.
20 S. Yang, M. Chu and Q. Miao, *J. Mater. Chem. C*, 2018, **6**, 3651–3657.
21 T. Nishinaga, T. Ohmae and M. Iyoda, *Symmetry*, 2010, **2**, 76–97.
22 W. Chen, H. Li, J. R. Widawsky, C. Appayee, L. Venkataraman and R. Breslow, *J. Am. Chem. Soc.*, 2014, **136**, 918–920.
23 Y. C. Teo, Z. Jin and Y. Xia, *Org. Lett.*, 2018, **20**, 3300–3304.
24 S. Hünig and H. Pütter, *Angew. Chem., Int. Ed. Engl.*, 1972, **11**, 431–432.
25 W. G. Shuler, S. P. Parvathaneni, J. B. Rodriguez, T. N. Lewis, A. J. Berges, C. J. Bardeen and M. J. Krische, *Chem. – Eur. J.*, 2021, **27**, 4898–4902.
26 W. Chen, F. Yu, Q. Xu, G. Zhou and Q. Zhang, *Adv. Sci.*, 2020, **7**, 1903766.
27 Z. Zhang and Q. Zhang, *Mater. Chem. Front.*, 2020, **4**, 3419–3432.
28 Q. Zhang, Y. Divayana, J. Xiao, Z. Wang, E. R. T. Tiekink, H. M. Doung, H. Zhang, F. Boey, X. W. Sun and F. Wudl, *Chem. – Eur. J.*, 2010, **16**, 7422–7426.
29 (*a*) Q. Zhang, J. Xiao, Z. Yin, H. M. Duong, F. Qiao, F. Boey, X. Hu, H. Zhang and F. Wudl, *Chem. – Asian J.*, 2011, **6**, 856–862; (*b*) J. Xiao, C. D. Malliakas, Y. Liu, F. Zhou, G. Li, H. Su, M. G. Kanatzidis, F. Wudl and Q. Zhang, *Chem. – Asian J.*, 2012, **7**, 672–675.

30 G. Li, H. M. Duong, Z. Zhang, J. Xiao, L. Liu, Y. Zhao, H. Zhang, F. Huo, S. Li, J. Ma, F. Wudl and Q. Zhang, *Chem. Commun.*, 2012, **48**, 5974–5976.
31 Y. Wu, Z. Yin, J. Xiao, Y. Liu, F. Wei, K. J. Tan, C. Kloc, L. Huang, Q. Yan, F. Hu, H. Zhang and Q. Zhang, *ACS Appl. Mater. Interfaces*, 2012, **4**, 1883–1886.
32 G. Li, Y. Wu, J. Gao, J. Li, Y. Zhao and Q. Zhang, *Chem. – Asian J.*, 2013, **8**, 1574–1578.
33 W. Chen, X. Li, G. Long, Y. Li, R. Ganguly, M. Zhang, N. Aratani, H. Yamada, M. Liu and Q. Zhang, *Angew. Chem., Int. Ed.*, 2018, **57**, 13555–13559.
34 J. Xiao, B. Yang, J. I. Wong, Y. Liu, F. Wei, K. J. Tan, X. Teng, Y. Wu, L. Huang, C. Kloc, F. Boey, J. Ma, H. Zhang, H. Y. Yang and Q. Zhang, *Org. Lett.*, 2011, **13**, 3004–3007.
35 J. Xiao, H. Yang, Z. Yin, J. Guo, F. Boey, H. Zhang and Q. Zhang, *J. Mater. Chem.*, 2011, **21**, 1423–1427.
36 B. Yang, J. Xiao, J. I. Wong, J. Guo, Y. Wu, L. Ong, L. L. Lao, F. Boey, H. Zhang, H. Y. Yang and Q. Zhang, *J. Phys. Chem. C*, 2011, **115**, 7924–7927.
37 J. Duan, P.-y. Gu, J. Xiao, X. Shen, X. Liu, Y. Yi and Q. Zhang, *Chem. – Asian J.*, 2017, **12**, 638–642.
38 U. H. F. Bunz, J. U. Engelhart, B. D. Lindner and M. Schaffroth, *Angew. Chem., Int. Ed.*, 2013, **52**, 3810–3821.
39 U. H. F. Bunz and J. Freudenberg, *Acc. Chem. Res.*, 2019, **52**, 1575–1587.
40 M. Schaffroth, R. Gershoni-Poranne, A. Stanger and U. H. Bunz, *J. Org. Chem.*, 2014, **79**, 11644–11650.
41 P. Biegger, M. Schaffroth, C. Patze, O. Tverskoy, F. Rominger and U. H. F. Bunz, *Chem. – Eur. J.*, 2015, **21**, 7048–7052.
42 P. Biegger, M. Schaffroth, O. Tverskoy, F. Rominger and U. H. F. Bunz, *Chem. – Eur. J.*, 2016, **22**, 15896–15901.
43 S. Yang, B. Shan, X. Xu and Q. Miao, *Chem. – Eur. J.*, 2016, **22**, 6637–6642.
44 S. Hünig and H. Pütter, *Angew. Chem., Int. Ed. Engl.*, 1972, **11**, 433.
45 M. P. Cava, D. R. Napier and R. J. Pohl, *J. Am. Chem. Soc.*, 1963, **85**, 2076–2080.
46 J. W. Barton, M. C. Goodland, K. J. Gould, J. Hadley and J. F. W. McOmie, *Tetrahedron*, 1978, **34**, 495–498.
47 E. Kolvari, M. A. Zolfigol, N. Koukabi, M. Gilandust and A.-V. Kordi, *J. Am. Chem. Soc.*, 2013, **10**, 1183–1191.
48 J. M. Blatchly, J. F. W. McOmie and S. D. Thatte, *J. Chem. Soc.*, 1962, 5090–5095.
49 A. L. Appleton, S. M. Brombosz, S. Barlow, J. S. Sears, J.-L. Bredas, S. R. Marder and U. H. F. Bunz, *Nat. Commun.*, 2010, **1**, 91.
50 M. Chu, J.-X. Fan, S. Yang, D. Liu, C. F. Ng, H. Dong, A.-M. Ren and Q. Miao, *Adv. Mater.*, 2018, **30**, 1803467.
51 S. Yang, D. Liu, X. Xu and Q. Miao, *Chem. Commun.*, 2015, **51**, 4275–4278.
52 M. Rosenberg, C. Dahlstrand, K. Kilså and H. Ottosson, *Chem. Rev.*, 2014, **114**, 5379–5425.
53 F. Ding, D. Xia, C. Ge, Z. Kang, Y. Yang, R. Fan, K. Lin and X. Gao, *J. Mater. Chem. C*, 2019, **7**, 14314–14319.
54 X.-Y. Liu, Y.-J. Zhang, X. Fei, Q. Ran, M.-K. Fung and J. Fan, *J. Mater. Chem. C*, 2019, **7**, 1370–1378.
55 L. Ahrens, J. Butscher, V. Brosius, F. Rominger, J. Freudenberg, Y. Vaynzof and U. H. F. Bunz, *Chem. – Eur. J.*, 2019, **26**, 412–418.
56 V. Brosius, S. Weigold, N. Hippchen, F. Rominger, J. Freudenberg and U. H. F. Bunz, *Chem. – Eur. J.*, 2021, **27**, 10001–10005.
57 P.-Y. Gu, N. Wang, A. Wu, Z. Wang, M. Tian, Z. Fu, X. W. Sun and Q. Zhang, *Chem. – Asian J.*, 2016, **11**, 2135–2138.
58 M. Ganschow, S. Koser, M. Hodecker, F. Rominger, J. Freudenberg, A. Dreuw and U. H. F. Bunz, *Chem. – Eur. J.*, 2018, **24**, 13667–13675.
59 C. Tong, J. Chang, J. M. Tan, G. Dai, K.-W. Huang, H. S. O. Chan and C. Chi, *Org. Biomol. Chem.*, 2013, **11**, 5683–5691.
60 H. Liao, C. Xiao, M. K. Ravva, L. Yao, Y. Yu, Y. Yang, W. Zhang, L. Zhang, Z. Li, I. McCulloch and W. Yue, *ChemPlusChem*, 2019, **84**, 1257–1262.
61 P.-Y. Gu, F. Zhou, J. Gao, G. Li, C. Wang, Q.-F. Xu, Q. Zhang and J.-M. Lu, *J. Am. Chem. Soc.*, 2013, **135**, 14086–14089.
62 J. J. Dressler, Z. Zhou, J. L. Marshall, R. Kishi, S. Takamuku, Z. Wei, S. N. Spisak, M. Nakano, M. A. Petrukhina and M. M. Haley, *Angew. Chem., Int. Ed.*, 2017, **56**, 15363–15367.
63 Z. Y. Wang, Y. Z. Dai, L. Ding, B. W. Dong, S. D. Jiang, J. Y. Wang and J. Pei, *Angew. Chem., Int. Ed.*, 2021, **60**, 4594–4598.
64 B. Yuan, J. Zhuang, K. M. Kirmess, C. N. Bridgmohan, A. C. Whalley, L. Wang and K. N. Plunkett, *J. Org. Chem.*, 2016, **81**, 8312–8318.
65 G. E. Rudebusch and M. M. Haley, in *Polycyclic Arenes and Heteroarenes*, ed. Q. Miao, Wiley-VCH Verlag GmbH & Co. KGaA, Weinheim, 1st edn, 2016, **2**, pp. 37–60.
66 G. L. Eakins, J. S. Alford, B. J. Tiegs, B. E. Breyfogle and C. J. Stearman, *J. Phys. Org. Chem.*, 2011, **24**, 1119–1128.
67 K. Plunkett, *Synlett*, 2013, 898–902.
68 Z. Wang, B. Chen, J. Zhao, Q. Zhang, Z. Lin, J. Weng and W. Huang, *Dyes Pigm.*, 2021, **191**, 109365.
69 D. Jakobi, A. Schumann and R. Beckert, *Z. Naturforsch., B: J. Chem. Sci.*, 2018, **73**, 493–500.
70 S. Hahn, F. L. Geyer, S. Koser, O. Tverskoy, F. Rominger and U. H. F. Bunz, *J. Org. Chem.*, 2016, **81**, 8485–8494.
71 B. D. Rose, D. T. Chase, C. D. Weber, L. N. Zakharov, M. C. Lonergan and M. M. Haley, *Org. Lett.*, 2011, **13**, 2106–2109.
72 C. K. Frederickson and M. M. Haley, *J. Org. Chem.*, 2014, **79**, 11241–11245.
73 F. Ding, D. Xia, W. Sun, W. Chen, Y. Yang, K. Lin, F. Zhang and X. Guo, *Chem. – Eur. J.*, 2019, **25**, 15106–15111.
74 T. Nakagawa, D. Kumaki, J.-I. Nishida, S. Tokito and Y. Yamashita, *Chem. Mater.*, 2008, **20**, 2615–2617.
75 F. Ebel and W. Deuschel, *Chem. Ber.*, 1956, **89**, 2799–2807.
76 Y. Miyata, T. Minari, T. Nemoto, S. Isoda and K. Komatsu, *Org. Biomol. Chem.*, 2007, **5**, 2592–2598.
77 W.-C. Chen, Y. Yuan, Z.-L. Zhu, S.-F. Ni, Z.-Q. Jiang, L.-S. Liao, F.-L. Wong and C.-S. Lee, *Chem. Commun.*, 2018, **54**, 4541–4544.

78 L. Ahrens, Y. J. Hofstetter, B. Celik, J. F. Butscher, F. Rominger, J. Freudenberg, Y. Vaynzof and U. H. F. Bunz, *Org. Mater.*, 2021, **3**, 168–173.
79 H. Li, S. Sun, S. Mhaisalkar, M. T. Zin, Y. M. Lam and A. C. Grimsdale, *J. Mater. Chem. A*, 2014, **2**, 17925–17933.
80 P.-Y. Gu, N. Wang, C. Wang, Y. Zhou, G. Long, M. Tian, W. Chen, X. W. Sun, M. G. Kanatzidis and Q. Zhang, *J. Mater. Chem. A*, 2017, **5**, 7339–7344.
81 T. Jia, J. Zhang, K. Zhang, H. Tang, S. Dong, C.-H. Tan, X. Wang and F. Huang, *J. Mater. Chem. A*, 2021, **9**, 8975–8983.
82 A. B. Marco, D. Cortizo-Lacalle, C. Gozalvez, M. Olano, A. Atxabal, X. Sun, M. Melle-Franco, L. E. Hueso and A. Mateo-Alonso, *Chem. Commun.*, 2015, **51**, 10754–10757.
83 M. R. Nimlos, J. Filley and J. T. McKinnon, *J. Phys. Chem. A*, 2005, **109**, 9896–9903.
84 M. Murata, Y. Sugano, A. Wakamiya and Y. Murata, *Angew. Chem., Int. Ed.*, 2015, **54**, 9308–9312.
85 X. Cui, G. Zhang, L. Zhang and Z. Wang, *Dyes Pigm.*, 2019, **168**, 295–299.
86 A. H. Abdourazak, Z. Marcinow, H. E. Folsom, F. R. Fronczek, R. Sygula, A. Sygula and P. W. Rabideau, *Tetrahedron Lett.*, 1994, **35**, 3857–3860.
87 P.-Y. Gu, G. Liu, J. Zhao, N. Aratani, X. Ye, Y. Liu, H. Yamada, L. Nie, H. Zhang, J. Zhu, D.-S. Li and Q. Zhang, *J. Mater. Chem. C*, 2017, **5**, 8869–8874.
88 P.-Y. Gu, Z. Wang, F.-X. Xiao, Z. Lin, R. Song, Q.-F. Xu, J.-M. Lu, B. Liu and Q. Zhang, *Mater. Chem. Front.*, 2017, **1**, 495–498.
89 M. Hodecker, M. Ganschow, M. Abu-Odeh, U. H. F. Bunz and A. Dreuw, *ChemPhotoChem*, 2019, **3**, 755–762.
90 H. Pan, T. Song, X. Yin, P. Jin and J. Xiao, *Chem. – Eur. J.*, 2018, **24**, 6572–6579.
91 V. Brosius, M. Müller, J. Borstelmann, F. Rominger, J. Freudenberg and U. H. F. Bunz, *J. Org. Chem.*, 2019, **85**, 296–300.
92 S. A. Odom, S. R. Parkin and J. E. Anthony, *Org. Lett.*, 2003, **5**, 4245–4248.
93 M. M. Payne, S. R. Parkin and J. E. Anthony, *J. Am. Chem. Soc.*, 2005, **127**, 8028–8029.
94 J. J. Bryant, Y. Zhang, B. D. Lindner, E. A. Davey, A. L. Appleton, X. Qian and U. H. F. Bunz, *J. Org. Chem.*, 2012, **77**, 7479–7486.
95 S. Hahn, S. Koser, M. Hodecker, P. Seete, F. Rominger, O. Š. Miljanić, A. Dreuw and U. H. F. Bunz, *Chem. – Eur. J.*, 2018, **24**, 6968–6974.
96 Y. Goto, S. Omagari, R. Sato, T. Yamakado, R. Achiwa, N. Dey, K. Suga, M. Vacha and S. Saito, *J. Am. Chem. Soc.*, 2021, **143**, 14306–14313.
97 M. Stępień, E. Gońka, M. Żyła and N. Sprutta, *Chem. Rev.*, 2016, **117**, 3479–3716.
98 Q. Xiao-Ni, L.-R. Dang, W.-J. Qu, Y.-M. Zhang, H. Yao, Q. Lin and T.-B. Wei, *J. Mater. Chem. C*, 2020, **8**, 11308–11339.
99 A. T. Balaban, D. C. Oniciu and A. R. Katritzky, *Chem. Rev.*, 2004, **104**, 2777–2812.
100 P. Biegger, M. Schaffroth, K. Brödner, O. Tverskoy, F. Rominger and U. H. F. Bunz, *Chem. Commun.*, 2015, **51**, 14844–14847.
101 K. Zhao, F. Yu, W. Liu, Y. Huang, A. A. Said, Y. Li and Q. Zhang, *J. Org. Chem.*, 2019, **85**, 101–107.
102 C. Wang, J. Wang, P.-Z. Li, J. Gao, S. Y. Tan, W.-W. Xiong, B. Hu, P. S. Lee, Y. Zhao and Q. Zhang, *Chem. – Asian J.*, 2014, **9**, 779–783.
103 B. Sadowski, J. Klajn and D. T. Gryko, *Org. Biomol. Chem.*, 2016, **14**, 7804–7828.
104 Y. Yuan, K.-C. Lo, L. Szeto and W.-K. Chan, *J. Org. Chem.*, 2020, **85**, 6372–6379.
105 M. Elter, L. Ahrens, S. M. Luo, F. Rominger, J. Freudenberg, D. D. Cao and U. H. F. Bunz, *Chem. – Eur. J.*, 2021, **27**, 12284–12288.
106 K. Zhao, W. Liu, F. Yu, G. Long, A. A. Said, Z. Wang, W. Gao and Q. Zhang, *Chem. – Eur. J.*, 2020, **26**, 4220–4225.
107 F. E. Arnold, *J. Polym. Sci., Part A-1: Polym. Chem.*, 1970, **8**, 2079–2089.
108 F. L. Hedberg, F. E. Arnold and R. F. Kovar, *J. Polym. Sci., Polym. Chem. Ed.*, 1974, **12**, 1925–1931.
109 G. Li, J. Gao, F. Hu and Q. Zhang, *Tetrahedron Lett.*, 2014, **55**, 282–285.
110 P.-Y. Gu, J. Gao, C.-J. Lu, W. Chen, C. Wang, G. Li, F. Zhou, Q.-F. Xu, J.-M. Lu and Q. Zhang, *Mater. Horiz.*, 2014, **1**, 446–451.
111 G. Li, G. Long, W. Chen, F. Hu, Y. Chen and Q. Zhang, *Asian J. Chem.*, 2013, **2**, 852–856.
112 G. Li, K. Zheng, C. Wang, K. S. Leck, F. Hu, X. W. Sun and Q. Zhang, *ACS Appl. Mater. Interfaces*, 2013, **5**, 6458–6462.
113 F. M. Jradi, M. H. Al-Sayah and B. R. Kaafarani, *Tetrahedron Lett.*, 2008, **49**, 238–242.
114 A. Fonari, F. M. Jradi, M. S. Fonari, M. H. Al-Sayah, M. Y. Antipin, B. R. Kaafarani and T. V. Timofeeva, *J. Mol. Struct.*, 2011, **996**, 141–147.
115 F. M. Jradi, A. a. O. El-Ballouli, M. H. Al-Sayah and B. R. Kaafarani, *Supramol. Chem.*, 2013, **26**, 15–24.